ORIGINAL PAPER

The Toarcian Posidonia Shale at Salem (North Alpine Foreland Basin; South Germany): hydrocarbon potential and paleogeography

Stephen Ajuaba[1] · Reinhard F. Sachsenhofer[1] · Francesca Galasso[2,3] · Thorsten U. Garlichs[5,6] · Doris Gross[1,4] · Elke Schneebeli-Hermann[2] · David Misch[1] · Jonathan E. Oriabure[1]

Abstract

The Posidonia Shale in the basement of the North Alpine Foreland Basin of southwestern Germany represents an important archive for environmental changes during the Toarcian oceanic anoxic event and the associated carbon isotope excursion (T-CIE). It is also an important hydrocarbon source rock. In the Salem borehole, the Posidonia Shale is ~ 10 m thick. The lower 7.5 m (1763.5–1756.0 m) of the Posidonian Shale and the uppermost part of the underlying Amaltheenton Formation were cored and studied using a total of 62 samples. Rock–Eval, palynological, maceral, biomarker and carbon isotope data were collected to assess variations in environmental conditions and to quantify the source rock potential. In contrast to most other Toarcian sections in southwest Germany, TOC contents are high in sediments deposited during the T-CIE, but reach a peak in post-CIE sediments. Biomarker ratios suggest that this reflects strong oxygen-depletion during the T-CIE (*elegantulum* to lower *elegans* subzones), but also during the *falciferum* Subzone, which is also reflected by a prolonged dinoflagellate cyst blackout. While sediments of the *tenuicostatum* Zone to the *elegans* Subzone are thinner than in neighbouring sections (e.g., Dotternhausen), sediments of the *falciferum* Subzone are unusually thick, suggesting that increased subsidence might have contributed to anoxia. The T-CIE interval is very thin (0.75 m). $\delta^{13}C$ values of *n*-alkanes show that the maximum negative isotope shift predates the strongest basin restriction during the T-CIE and that the carbon isotope shift is recorded earlier for aquatic than for terrigenous organisms. In Salem, the Posidonia Shale is thermally mature and highly oil-prone. The residual source petroleum potential is about 0.8 tHC/m^2.

✉ Stephen Ajuaba
  stephen.ajuaba@unileoben.ac.at

1 Chair of Energy Geosciences, Montanuniversitaet Leoben, Peter-Tunner-Strasse 5, 8700 Leoben, Austria

2 Paläontologisches Institut und Museum, Universität Zürich, Karl-Schmid-Strasse 4, 8001 Zurich, Switzerland

3 Present Address: Senckenberg Forschungsinstitut und Naturmuseum Frankfurt, Senckenberganlage 25, 60325 Frankfurt am Main, Germany

4 Present Address: Sandvik Mining and Construction G.m.b.H., Alpinestrasse 1, 8740 Zeltweg, Austria

5 Wintershall Dea Norge AS, Jåttåflaten 27, 4020 Stavanger, Norway

6 Wintershall Dea Norge AS, PO Box 230 Sentrum, 4001 Stavanger, Norway

Introduction

Oceanic anoxic events are important features of the Mesozoic Era (e.g., Schlanger and Jenkyns 1976; Jenkyns 2010). The Toarcian oceanic anoxic event (T-OAE; ~ 183 Ma) is the oldest of these Mesozoic events (Jenkyns 1985, 1988). It is characterised by global climate change (Ruebsam and Schwark 2021 and references therein), mass extinction of marine biota (e.g., Harries and Little 1999; Pálfy and Smith 2000; Dera et al. 2010; Caruthers et al. 2013), and a prominent negative carbon isotope shift (3–8‰) referred to as the Toarcian Carbon Isotope Excursion (T-CIE) (e.g., Hesselbo et al. 2000, 2007).

While records of the T-OAE are found globally (e.g., Jenkyns et al. 2001; Chen et al. 2023), the most organic-rich sediments related to the T-OAE occur in the epicontinental Central European Basin (CEB) of Britain, Germany,

Switzerland, and France (Fig. 1a; e.g., Küspert 1982; Littke et al. 1991a, b; Baudin 1995; Jenkyns and Clayton 1997; Röhl et al. 2001). In Germany and Switzerland, the Toarcian black shales are called Posidonia Shale.

In southern Germany and Switzerland, the Posidonia Shale has been described in detail in the Swabian and Franconian Alb (e.g., Riegraf et al. 1984; Riegraf 1985; Röhl et al. 2001; Röhl and Schmid-Röhl 2005; Hougård et al. 2021) and the Swiss Jura (Kuhn and Etter 1994;
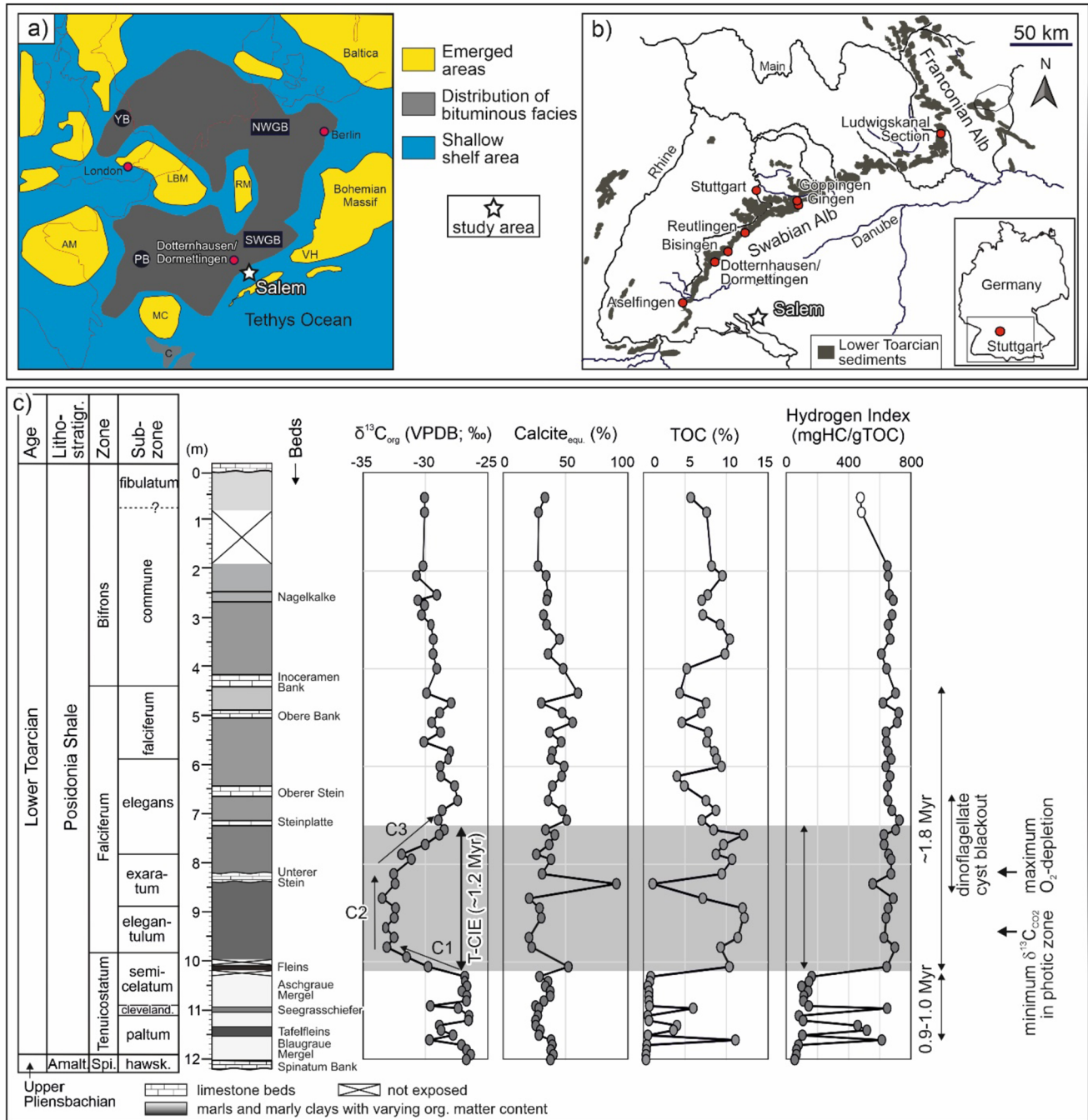

Fig. 1 a Early Toarcian paleogeography of the epicontinental Central European Basin with the distribution of bituminous black shale across various sub-basins (*SWGB* SW German Basin, *NWGB* NW German Basin, *YB* Yorkshire Basin and *PB* Paris Basin); **b** outcrops of the lower Toarcian sediments in southwestern Germany. The white star indicates the study area (Salem). Maps are modified after Ziegler (1982), Röhl et al. (2001), and Galasso et al. (2021). **c** Stratigraphy, isotope data, and bulk geochemical data of the Dormettingen section (after Galasso et al. 2021, 2022; Ajuaba et al. 2022). The duration of the *tenuicostatum* and *falciferum* zones and of the T-CIE follows Ruebsam et al. (2023). HI values of weathered samples near the top of the succession are shown with open symbols

Montero-Serrano et al. 2015; Fantasia et al. 2019) (Fig. 1b). Here, the oil-prone Toarcian sediments are thermally immature or marginal mature (Littke et al. 1991b), which is favorable for applying organic parameters (e.g., biomarkers) to reconstruct the depositional environment.

The most comprehensive data in the area are available for the Dotternhausen and Dormettingen sections, which are only ~2 km apart (Fig. 1a, b). Both sections haves been studied in great detail using different sedimentological, paleontological, and geochemical techniques (e.g., Riegraf 1985; Schouten et al. 2000; Röhl et al. 2001; Frimmel et al. 2004; Schwark and Frimmel 2004; Röhl and Schmid-Röhl 2005, van de Schootbrugge et al. 2005; Bour et al. 2007; Mattioli et al. 2008; Suan et al. 2008, 2015; Wang et al. 2020, 2021; Galasso et al. 2021, 2022; Ajuaba et al. 2022; Reubsam et al. 2023).

The present study is based on core material from the "Salem A" borehole (in the following called Salem borehole), drilled in the German part of the North Alpine Foreland Basin, about 65 km southeast of Dormettingen. In this borehole, Toarcian black shales have been noted between 1753 and 1763 m depth and are overlain by younger Jurassic and Cenozoic sediments. Based on the considerable depth, it is likely that the Posidonia Shale is thermally mature (cf., Wehner and Kuckelkorn 1985). Moreover, its location close to Vindelician High (e.g., Riegraf 1985; Meyer and Schmidt-Kahler 1996) suggests deposition at shallower water depth than at Dormettingen. Consequently, the examination of the Salem drill core presents an opportunity to explore variations in sedimentary facies between the proximal Salem location and the more distal Dormettingen/Dotternhausen sites. In addition, it provides a means to investigate the impact of increasing thermal maturity on organofacies characteristics, a particularly pertinent aspect when utilising biomarker data for establishing connections between oil and its source.

Geological setting

Sediments with very high total organic carbon (TOC) contents were deposited during early Toarcian time in the epicontinental CEB (Fig. 1a; Ziegler 1982, 1988). Black shale deposition in the Yorkshire Basin (Hesselbo et al. 2000; Bowden et al. 2006; Kemp et al. 2011; French et al. 2014), the Northwest German Basin (e.g., Littke et al. 1991a), the Southwest German Basin, and the Paris Basin (Hollander et al. 1991; Hermoso et al. 2009, 2014; Song et al. 2014) was controlled by strong oxygen-depletion due to climate change (T-OAE; Jenkyns 1985, 1988), water column stratification (e.g. Küspert 1982; Röhl et al. 2001; Schwark and Frimmel 2004; Hermoso et al. 2013; Song et al. 2015, 2017),

and eustatic sea level variations (see Ruebsam and Schwark 2021 for a review).

The studied drill core originates from the Southwest German Basin (SWGB). The Dotternhausen and Dormettingen quarries provide key sections for this part of the CEB. Some key parameters are displayed for the Dormettingen section in Fig. 1c. At Dormettingen, the lower Toarcian sediments overlie bioturbated marls assigned to the Pliensbachian Amaltheenton Formation (*Pleuroceras spinatum* Zone) intercalated with a tens of cm thick limestone bed ("Spinatum-Bank" or "Costaten-Kalk"). The approximately 12-m thick Posidonia Shale Formation overlies the Amaltheenton Formation without indication of a sedimentary gap (Galasso et al. 2021) and includes the *Dactylioceras tenuicostatum* zone, the *Harpoceras falciferum* and *Hildoceras bifrons* zones (Riegraf 1985; Röhl et al. 2001; Röhl and Schmid-Röhl 2005). Light-grey bioturbated marls and 3 several-cm-thick black shale layers (Tafelfleins, Seegrasschiefer, and Fleins) occur in the *tenuicostatum* Zone. The Fleins forms the base of massive black shales deposit representing the T-OAE (uppermost *tenuicostatum, falciferum* and *bifrons* zones; Fig. 1c). Prominent limestone beds are intercalated into the black shale succession and are labelled from base to top: "Unterer Stein" (20–30 cm thick; *exaratum* Subzone), "Steinplatte" (~10 cm thick; *elegans* Subzone), "Oberer Stein" (~20 cm thick; *elegans* Subzone), "Obere Bank" (~10 cm thick; *falciferum* Subzone) and "Inoceramen Bank" (~10 cm thick; boundary between *falciferum and bifrons* zones). The Toarcian carbon isotope excursion (T-CIE; ~183 million years; Myr) extends from the Fleins Bed to the "Steinplatte" and spans an interval of 2.8 m at Dormettingen/Dotternhausen (Suan et al. 2008; Galasso et al. 2021; Ajuaba et al. 2022).

Using an astronomical timescale, Ruebsam et al. (2023) estimated the duration of the *tenuicostatum* and *falciferum* zones as 0.9–1.0 and 1.8 Myr, respectively (cf. Fig. 1c). The duration of the T-CIE (*elegantulum* to lower *elegans* Subzones of the *falciferum* Zone) has been estimated as 0.9 (Suan et al. 2008) or 1.2 Myr (Ruebsam et al. 2023). The carbon sources that caused the T-CIE are discussed controversially and may include CO_2 or methane emitted from the Karoo-Ferrar Large Igneous Province (e.g., Pálfy and Smith 2000; McElwain et al. 2005; Svensen et al. 2007) or methane emissions from marine gas hydrates (Hesselbo et al. 2000; Kemp et al. 2005), wetlands (Them et al. 2017) and permafrost areas (Ruebsam et al. 2019).

The Dotternhausen and Dormettingen sections occupied central positions within the SWGB (e.g., Riegraf et al. 1985). In contrast, the Salem drill site is located near the southeastern basin margin, where the SWGB was separated from the Tethys Ocean by a series of islands forming the continuation of the Vindelician High (Fig. 1a).

Samples and analytical methods

Samples

This present study is based on 62 samples collected from a 9-m-long drill core recovered from the Salem borehole drilled by Wintershall in the 1970s. The core is stored in ten core boxes. A photograph of nine of them is shown in Fig. 2a. The samples originate from the Upper Pliensbachian Amaltheenton Formation (8 samples) and the Lower Toarcian Posidonia Shale (54 samples). Samples were collected in varying intervals ranging from 1 to 63 cm. To obtain a high-resolution record of the T-CIE, the sampling interval was especially small in the interval between 1762.5 and 1761.3 m. The sample ID reflects the depth in meter (e.g., #1765.20 is the sample from 1765.20 m depth).

Analytical methods

Computed tomography (CT) scans were performed at the Chair of Reservoir Engineering, Montanuniversitaet Leoben. Geochemical and maceral analyses were performed at the

Fig. 2 **a** Photograph of nine boxes with the upper 8 m(!) of the Salem drill core. Note that the box with the lowermost core meter is not shown. The diameter of the core is 10 cm. The depth decreases from the left lower to the right upper corner. The position of marker beds, samples (green dots) and the T-CIE (red bar) are indicated together with the location of core pieces shown in the lower part of the figure. **b** Spinatum Bank with interlayering marl. **c**, **d** Detail of the Tafelfleins with distinct bioturbation structures (*Chonchites*); a belemenite rostrum is visible in sediments overlying the Tafelfleins, **e** "Unterer Stein" marker bed. **f** Imprints of shells (Bositra). **g** Core interval with abundant belemnite remains. *Unt.St.* Unterer Stein
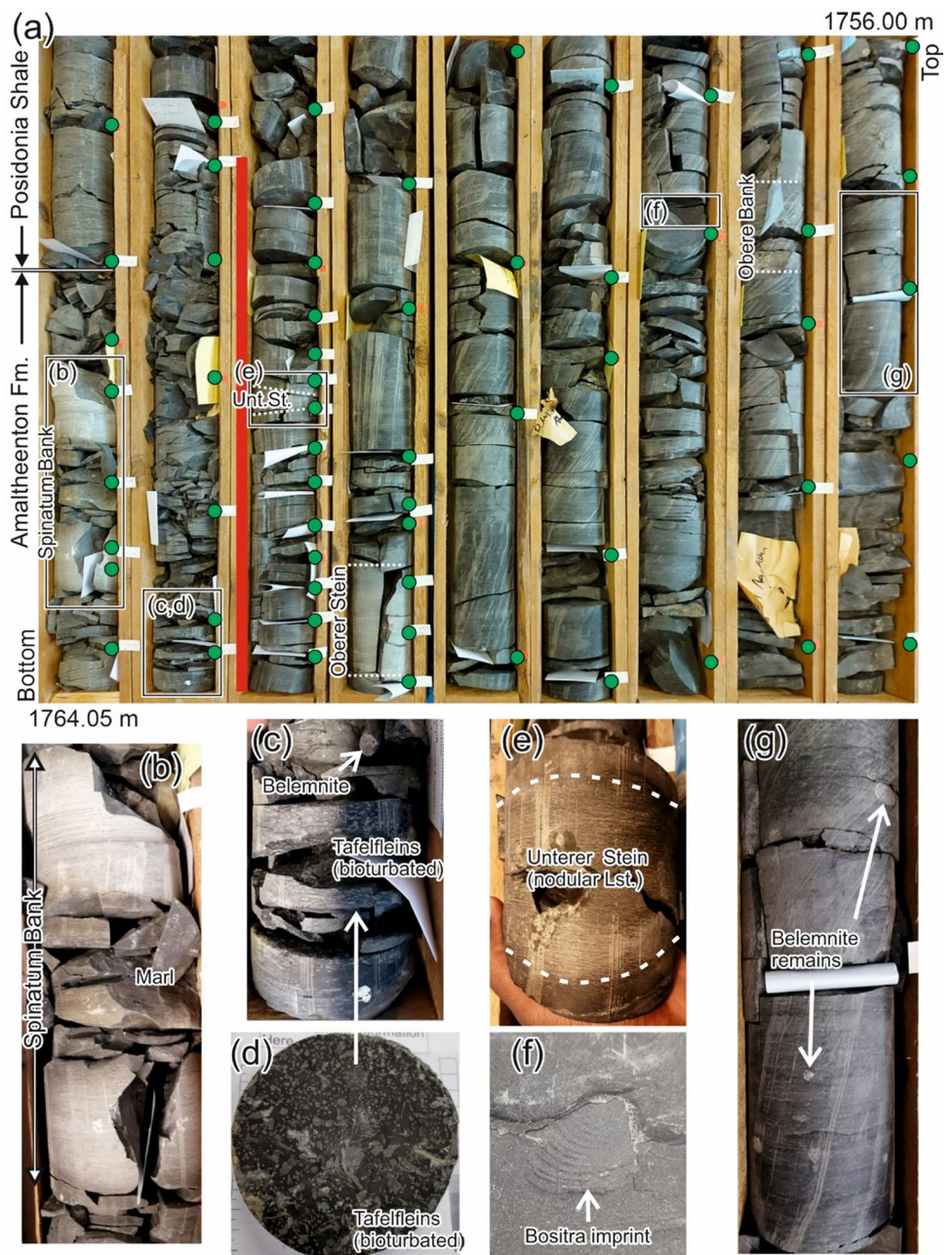
laboratories of the Chair of Energy Geosciences at Montanuniversitaet Leoben. Palynological investigations were conducted at the Paläontologisches Institut und Museum, Universität Zürich.

Computed tomography (CT) Scan

The upper 8 m of the drill core were scanned with Siemens Somatom Definition AS, a medical CT scanner at a resolution of 0.3×0.3 mm in the xy plane and 0.6 mm in the z direction, to image density contrast and to detect pyrite, shells, belemnites, etc. along the studied stratigraphic section.

Bulk geochemistry

All samples were powdered for bulk geochemical analysis. For the bulk organic carbon isotope ($\delta^{13}C_{org}$) analysis, 58 samples with total organic carbon (TOC) contents > 0.15 wt% were pre-treated step-wise with 6 N HCl for almost 12 h to remove all carbonates. Distilled water was used at each step to remove the added acid. The samples were later oven dried for 24 h at 40 °C. For each sample, 6–8 mg was weighed into tin-foil boats and measured by combustion in excess of oxygen at 1020 °C using an elemental analyzer (Flash EA 1112). The CO_2 by-product is separated by column chromatography and analysed online by the DELTA V ir-MS. The carbon isotopic ratio ($^{13}C/^{12}C$) of the sample CO_2 are compared with that of the CO_2 reference gas and calibrated against PDB. Analytical reproducibility is in the range of 0.1–0.3‰.

All 62 samples were analysed twice for total carbon (TC; wt%), total sulphur (TS; wt%) and total organic carbon (TOC; wt%) contents using an Eltra Helios CS elemental analyzer. For the analysis, the samples were combusted in an oxygen atmosphere at 1350 °C and the resulting carbon and sulphur dioxides were measured by an infrared detector. TOC contents were measured on samples pre-treated with concentrated phosphoric acid to remove carbonate minerals. Consequently, the difference between TC and TOC is the amount of total inorganic carbon (TIC). Calcite equivalent percentages were derived assuming that calcite is the only carbonate mineral present (calcite$_{equiv.}$ = 8.334 × TIC).

A "Rock–Eval 6" instrument was used to determine S_1, S_2, [mgHC/g rock] and T_{max} [°C] for all samples in duplicate. Hydrocarbons volatized from the sample at 300 °C form the S_1 peak, while hydrocarbons generated during gradual heating from 300 to 650 °C form the S_2 peak. T_{max} is the temperature of maximum hydrocarbon generation corrected to Rock–Eval standards. Calculated parameters include hydrogen index (HI = 100 × S_2/TOC), production index (PI = S_1/[S_1 + S_2]) and genetic potential (GP = S_1 + S_2) (Espitalié et al. 1977).

Different subsets of these samples were selected based on their TOC content and their stratigraphic position for maceral, palynology, biomarker, and stable carbon isotope analysis.

Particulate organic matter and palynology

Fourteen samples, representing different units in the Posidonia Shale including organic-lean sediments below the T-CIE, were selected to determine the origin and preservation state of particulate organic matter. About 15 g of dry sediment was cleaned, crushed, and subsequently treated with concentrated HCl and HCF to obtain kerogen concentrates. Kerogen concentrates were oxidised with nitric acid or Schulze's solution as described by Traverse (2007) to remove pyrite. After mineral dissolution and after oxidation, the residues were sieved over a 11-µm mesh screen. For palynofacies analysis, organic matter particles were counted in unoxidised kerogen slides until a minimum of 400 counts per sample was reached. Particle counts include marine particles [i.e. acritarchs, prasinophytes, amorphous organic matter (AOM), foraminiferal test linings and dinoflagellate cysts] and terrestrial particles (i.e. translucent and opaque phytoclasts, cuticles, membranes, spores and bisaccate pollen grains) (Tyson 1995; Batten 1996). Subsequently, for a detailed palynological investigation, all samples were further treated (with a stepped process of oxidation) using concentrated HNO_3, and ultrasonic vibration. This treatment was done to increase the palynomorph concentration, remove the remaining inorganic residue (e.g. pyrite), and reduce the AOM density.

Organic petrography

Eleven samples were selected for organic petrological investigation. These samples are identical to those used for palynological studies, or they are located nearby. Semi-quantitative maceral analyses were performed on polished blocks using white and fluorescence light, a 50× oil immersion objective, and a Leica DM 4P microscope. Close to 1500 points were counted per sample and the results are normalized to 100% organic matter. This analysis was in accordance to the ICCP system (ICCP 1998, 2001; Pickel et al. 2017). Measurements of mean random vitrinite reflectance (%Rr) (Taylor et al. 1998) were performed in non-polarized light with a wavelength of 546 nm. The microscope was calibrated with a synthetic reflectance standard (N-LASF46A; Rr: 1.311%).

Biomarker analysis

Thirty-one samples representing the entire core interval were selected for biomarker analysis, with a particularly large number of samples taken from the T-CIE interval. For each sample, 5–10 g of material was extracted for about 1 h at 75 °C and 100 bar using dichloromethane as solvent and a Dionex ASE 350 Accelerated Solvent Extractor. The extract was concentrated to ~ 0.5 ml using a Zymark TurboVap 500 closed cell concentrator. Afterwards, asphalthenes were precipitated from a hexane:dichloromethane solution (80:1 according to volume) and separated by centrifugation. The hexane-soluble fractions were further separated into aliphatic, aromatic and heterocompounds (NSO) by medium-pressure liquid chromatography using a Köhnen-Willsch MPLC instrument (Radke et al. 1980). Proportionate amounts of internal standards (*n*-tetracosane or squalene for aliphatics and 1,1′-binaphthyl for aromatics) were added to each sample prior to measurement.

The *n*-alkanes and isoprenoids in the saturated hydrocarbon fractions were analysed using a gas chromatograph (Trace GC-Ultra) with a flame ionization detector (GC-FID). The GC was equipped with a 50 m HP-PONA capillary column (inner diameter [i.d] 0.2 mm, 0.50 μm film thickness). After splitless sample injection at 270 °C, the oven temperature was increased from 70 to 310 °C followed by 35 min isothermal period.

Specific biomarker molecules in the saturated and aromatic fractions were analysed by gas chromatography-mass spectrometry (GC–MS) using a Thermo Scientific Trace GC-Ultra equipped with a 60 m TG/DB-5MS fused silica capillary column (i.d. 0.25 mm; 0.25 μm film thickness) coupled to ThermoFisher ISQ mass spectrometer. The GC oven temperature was initially programed from 40 °C/min (held for 2 min) and increased to 310 °C with 4 °C/min followed by an isothermal period of 40 min. Samples were injected in split mode with a split ratio of 20 at 260 °C using helium as carrier gas. The spectrometer was operated in the EI (electron ionization) mode with a mass-to-charge ratio (*m/z*) scan range from m/z 50 to m/z 650 (0.7 s total scan time). For the determination of methylsterane concentrations, further investigating aliphatic fractions of selected samples using a Trace™ 1300 GC (ThermoFisher) equipped with a 60 m TG-5MS fused silica capillary column (i.e. 0.25 mm; 0.25 μm film thickness) attached to a ThermoFisher TSQ9000 triple quadrupole GC–MS/MS. The oven was set to hold 40 °C for 2 min and then heated to 310 °C with 4 °C/min, followed by a constant temperature period of 40 min. The sample was injected splitless with an injector temperature of 310 °C. Methylsterane isomers were detected using selected reaction monitoring (SRM) through the application of different parent-to-daughter ion transitions (m/z 386–231, 400–231, 414–231, 414–98) to obtained C_{28} to C_{30} methylsteranes, methyldiasteranes, and dinosteranes.

The raw data were processed using Xcalibur and Chromeleon data systems. The respective retention time for each compound within the mass spectra or total ion current (TIC) were used for their identification in addition to comparing the mass spectra with published data. Correction factors were appropriately applied for mass chromatograms to correct for fragment ions while for TIC chromatograms, absolute concentrations were determined from the peak areas of the saturated and aromatic fractions in relation to their internal standards per sample.

A semi-quantitative calculation of the target compounds was conducted based on results of TIC chromatograms. Absolute concentrations were determined for the methylsteranes using their TIC chromatograms (also detectable using m/z 231) set in relation to an internal standard (5β(H)-Cholane) per sample.

Compound-specific carbon isotopy

To analyse the stable carbon isotope of *n*-alkanes and isoprenoids, the *n*-alkanes were separated from the *iso*-alkanes within the saturated hydrocarbon fraction using an improved 5 Å molecular sieve method (Grice et al. 2008). Measurement of the stable carbon isotope ratio was performed using a Trace GC-Ultra gas chromatograph attached to the ThermoFisher Delta-V isotope ratio mass spectrometer (IRMS) via a combustion and high temperature reduction interface (GC Isolink, ThermoFisher). The GC column has been described above, however the oven temperature was set to 70 °C for 2 min followed by a ramp from 4 °C/min to 300 °C and isothermal period of 15 min. A CO_2 reference gas was used for calibration and injected before and after each analysis. Isotope composition per sample was measured at least twice and their mean values reported in the δ notation in permil (‰) relative to the V-PDB standard. The analytical reproducibility per sample is below 0.3‰.

Results

According to well logs, the lower Toarcian Posidonia Shale was drilled at Salem between 1753 and 1763 m depth (below surface). The present study is based on a drill core representing the depth interval from 1756 to 1765 m. Hence, no analytical data are available for the uppermost 3 m of the Posidonia Shale (1753–1756 m).

Bulk organic carbon isotope data ($\delta^{13}C_{org}$)

Bulk organic carbon isotope ratios are an important correlation tool for Pliensbachian and Toarcian sediments. Hence,

these ratios are presented first to provide a stratigraphic framework. $\delta^{13}C_{org}$ values in the studied interval vary between − 25.7 and − 33.1‰. Overall, they show a gradual upward decrease from ~ − 26 to − 29‰. Significantly lower ratios (− 28.5 to − 33.1‰) representing the T-CIE (*elegantulum* to lower *elegans* Subzones; Riegraf et al. 1984; Suan et al. 2008; 2015; Ruebsam and Al-Husseini 2020) are observed in a 0.75 m thick interval (1762.25–1761.50 m).

Lithology and stratigraphy

Sediments below the T-CIE belong to the upper Pliensbachian Amaltheenton Formation and the lower part of the Toarcian Posidonia Shale. The uppermost part of the Amaltheenton Formation is composed of light- to dark-grey bioturbated marls and two limestone layers ("Spinatum Bank"; Fig. 2b). The "Spinatum Bank" is overlain by bioturbated marls with low organic matter contents ("Blaugraue Mergel") and two organic matter-rich intervals, which contain the trace fossil *Chondrites* (Tafelfleins, Seegrasschiefer; Fig. 2c, d). Organic-lean sediments with some shell remains ("Aschgraue Mergel") follow above the Seegrasschiefer. Bituminous sediments, about 20 cm thick, occur immediately below the T-CIE and are correlated with the "Fleins" Bed at the base of the main black shale succession. Belemnite remains are present in the pre-CIE sediments (Fig. 2c), albeit in low quantities.

The Pliensbachian/Toarcian boundary (*spinatum/tenuicostatum subzones*) is located just above the Spinatum Bank and significantly below the first black shale layer (e.g., Riegraf 1985). For the Salem locality, this is approximately 10 cm above the Spinatum Bank (1763.50 m; Fig. 2a).

Black shales within the T-CIE (1762.25–1761.50 m) show a distinct lamination. A nodular limestone bed "Unterer Stein" is present in the middle part of the T-CIE (~ 1761.85 m; Fig. 2e). Black shales below the limestone marker contain a thin coaly layer and very low carbonate contents. Carbonate contents above the limestone marker are higher. Some shells are present in the uppermost part of the T-CIE, but belemnite remains have not been observed.

The sediments above the T-CIE are dominated by marly black shales with relatively high carbonate contents. Two distinct limestone layers are present (Figs. 2, 3). The layer at ~ 1761.2 m represents the "Oberer Stein", which is the best marker horizon in the SWGB (upper part of the *elegans* Subzone; Riegraf 1985). The layer at ~ 1756.9 m is the "Obere Bank", another wide-spread marker bed (upper part of the *falciferum* Subzone). Light bioturbation features are observed above the "Oberer Stein" (~ 1761.1 m), at about 1757.9 m and above the "Obere Bank" (~ 1756.5 m). In contrast, black shales with distinct lamination, locally containing pyrite veins and nodules, prevail in the middle part of the succession (1761.0–1757.9 m). Imprints of rare bivalves

are observed at ~ 1758.15 m (Fig. 2e). Belemnite remains are largely missing below 1760.6 m, but highly abundant in the uppermost part of the section above the "Obere Bank" (1756.5–1756.0 m, Figs. 2f, 3). The "Inoceramen Bank", which forms the boundary between the *falciferum and bifrons* zones (e.g., Fig. 1) is absent in the Salem core. This suggests that the uppermost part of the core still belongs to the *falciferum* Zone.

Bulk geochemistry

Calcite, TOC, and sulphur contents as well as Rock–Eval data are reported in this section (Fig. 3; Table 1). Carbonate contents decrease upwards from 61 wt% (#1764.90) in the Amaltheenton Formation to 15 wt% in the lower part of Posidonia Shale (#1762.08) and are significantly higher only in the Spinatum-Bank (#1763.85, #1763.83, #1763.63). Within the T-CIE, calcite contents are lower below the "Unterer Stein" (average: 18 wt%) and higher above of it (average 36 wt%). Calcite contents above the T-CIE are on average 44 wt%, but exceed 75 wt% in the "Oberer Stein" and the "Obere Bank".

The TOC contents within the Amaltheenton Formation are very low (< 0.3 wt%), while sulphur contents are moderate (0.08–1.12 wt%). HI values are generally low (average 73 mgHC/gTOC).

Below the T-CIE, organic matter richness (0.26–3.68 wt% TOC), sulphur content (0.56–3.39 wt%) and HI (59–470 mgHC/gTOC) vary strongly in the Posidonia Shale. High values are observed in the "Tafelfleins", the "Seegrasschiefer" and the black shale layer underlying the T-CIE.

As expected, the black shales within the T-CIE interval exhibit elevated TOC levels ranging from 4.78 to 7.44%, along with sulphur contents ranging from 2.41 to 4.50%. In contrast, the "Unterer Stein" limestone displays notably lower TOC and sulphur contents. The most substantial TOC concentrations, exceeding 7%, are found above the "Unterer Stein" while the highest sulphur contents, surpassing 4%, are observed below the "Unterer Stein". HI values are high (538–634 mgHC/gTOC) in all samples.

The black shales above the T-CIE show varying TOC contents which allow a subdivision of the sediments into various units. The succession starts with an interval (unit I: 1761.50–1761.00 m) with moderate TOC contents (2.73–4.48 wt%) and HI values varying from 455 to 630 mgHC/gTOC. Sulphur contents are relatively uniform (1.50–1.87%). The overlying unit II (1761.99–1757.92 m) contains very high TOC contents (4.71–8.95%) with a subtle slightly decreasing upwards, uniformly high HI values (557–660 mgHC/gTOC), and partly very high sulphur contents (1.02–4.31). TOC contents are only moderately high (2.92–4.04%) in unit III (1757.9–1757.0 m), while HI (462–523 mgHC/gTOC) and sulphur contents
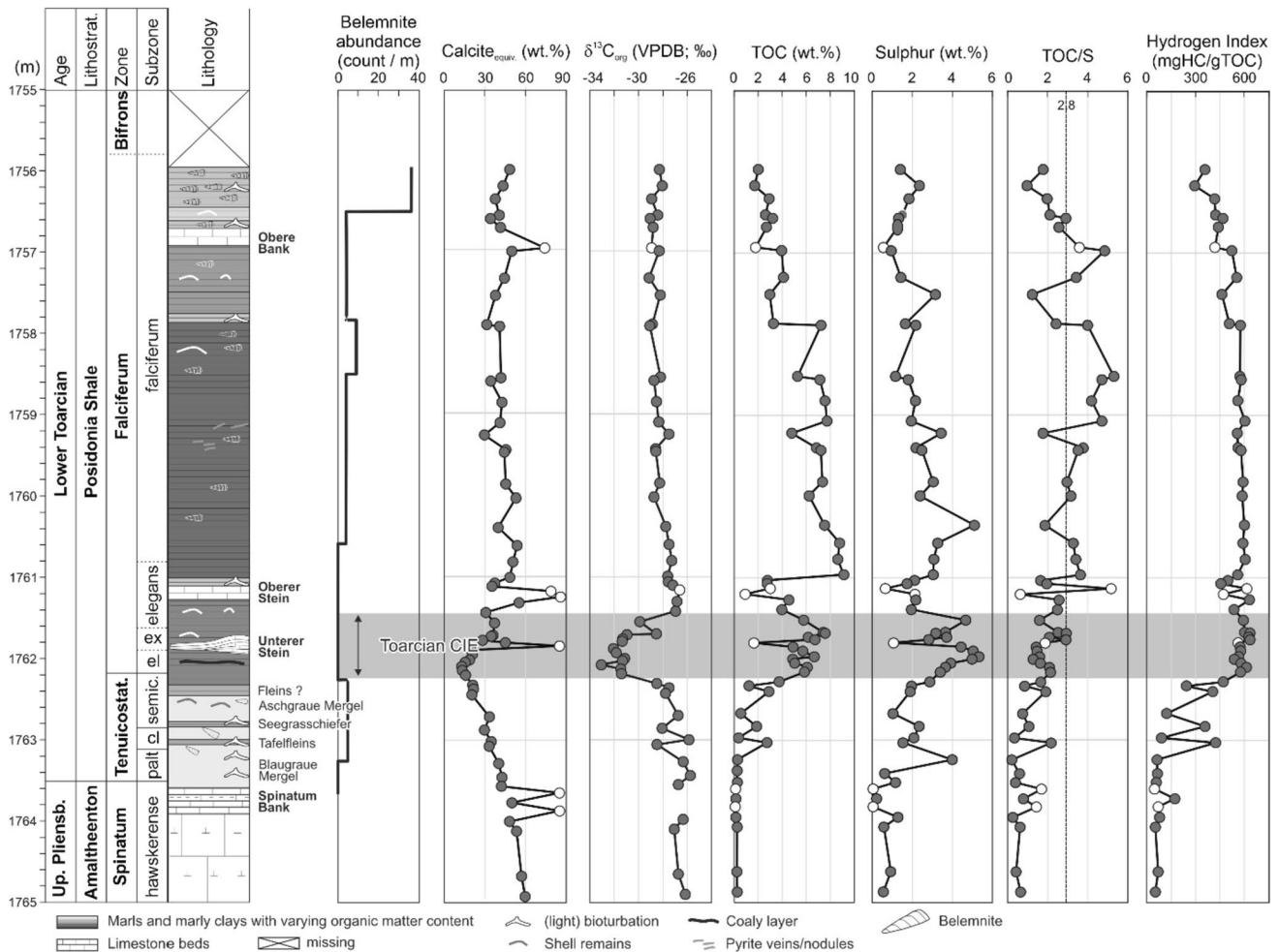
Fig. 3 Stratigraphic profile across the Salem drill core with ammonite zones; belemnite counts (obtained from CT scans; lowermost 1 m was not available for scanning), calcite equivalent percentage; bulk organic carbon isotope trend; d) total organic carbon (TOC); sulphur contents, TOC/S ratios, and hydrogen index. Open symbols represent data points from limestone samples

(0.84–2.69%) are also reduced. The uppermost interval (1756.96–1755.0 m; unit IV) is characterized by relatively low TOC contents (1.68–3.16%), HI values (296–464 mgHC/gTOC) and sulphur contents ranging from 1.11 to 2.02% and are lower than in unit III. The limestone marker beds in unit I ("Oberer Stein") and at the base of unit IV ("Obere Bank") contain low TOC and sulphur contents, but HI values are similar to those in adjacent black shales.

Across the entire study section, TOC/S ratios vary significantly, but show a general upward increase from the base of the Posidonia Shale (~1.0) to a depth of 1757.92 m (~4.5). Above a minimum (1.02) at 1757.54 m, TOC/S ratios decrease upwards between 1757.0 and 1756.0 m from ~4.7 to 1.0.

T_{max} values of samples with $S_2 > 1.0$ mgHC/grock vary from 431 to 439 °C (average 436 °C) (Table 1). The average PI for black shales (TOC > 1.0 wt%) and organic-lean sediments (TOC < 1.0 wt%) is 0.08 and 0.23, respectively.

Palynofacies

The particulate organic matter (POM) shows three intervals (from base to top: A to C) with distinctive compositions (Fig. 4).

Interval A includes two organic-lean (#1763.00; #1762.70) and one organic-rich sample (#1762.43) from the Posidonia Shale below T-CIE. The POM assemblage is marked by a conspicuous amount of opaque phytoclasts and a high occurrence of palynomorphs. Acritarchs, dinoflagellate cysts and AOM contributed 1.23%, 0.26% and 76.31% POM on average respectively (Table 2; Fig. 4).

Interval B is documented for samples from the T-CIE (#1762.03; #1761.70) and the lower part of the post-CIE sediments (#1761.10 to #1759.10 m). It is characterised by a strong increase in AOM. With the exception of the lowermost sample (#1762.03), the terrigenous fraction (e.g., translucent phytoclasts, spores) is extremely reduced. However,

Table 1 Bulk geochemical parameters for samples from the Salem drill core

Sample ID (m)	Calcite (wt%)	TOC (wt%)	Sulphur (wt%)	TOC/S (–)	S$_1$	S$_2$ (mg HC/g rock)	HI (mg HC/g TOC)	T_{max} (°C)	PI (–)	GP (mg HC/g rock)	$\delta^{13}C_{org}$ (VPDB; ‰)	
#1756.00	49.74	1.98	1.22	1.62	0.44	7.10	358	435	0.06	7.54	− 28.28	Post-CIE
#1756.20	44.91	1.68	2.02	0.83	0.35	4.95	295	434	0.07	5.30	− 28.05	
#1756.36	39.09	2.88	1.58	1.82	0.74	12.01	417	435	0.06	12.75	− 28.92	
#1756.56	42.14	2.56	1.31	1.96	0.74	10.83	423	434	0.06	11.56	− 28.42	
#1756.60	35.59	3.16	1.15	2.74	0.72	14.76	468	438	0.05	15.48	− 29.04	
#1756.71	42.97	2.65	1.11	2.40	0.90	11.68	440	436	0.07	12.57	− 28.79	
#1756.96	75.58	1.76	0.52	3.41	0.75	7.38	419	432	0.09	8.12	− 28.92	
#1757.00	51.24	3.89	0.84	4.65	1.85	20.38	523	435	0.08	22.23	− 28.30	
#1757.33	45.84	4.04	1.24	3.25	1.44	22.32	553	436	0.06	23.76	− 29.13	
#1757.54	39.30	2.92	2.69	1.09	1.35	13.52	462	436	0.09	14.87	− 28.21	
#1757.90	32.91	3.22	1.43	2.26	1.23	16.39	508	434	0.07	17.62	− 28.85	
#1757.92	42.34	7.10	1.87	3.81	3.78	40.84	575	438	0.08	44.62	− 29.06	
#1758.55	43.34	5.18	1.02	5.10	4.00	29.68	573	438	0.12	33.68	− 28.20	
#1758.59	35.79	7.01	1.55	4.51	3.37	40.65	580	439	0.08	44.02	− 28.72	
#1758.85	44.12	7.42	1.85	4.00	3.93	41.57	660	437	0.09	45.50	− 28.52	
#1759.10	42.60	7.58	1.68	4.51	4.24	45.71	603	436	0.08	49.95	− 28.34	
#1759.25	31.16	4.71	2.93	1.61	2.53	26.23	557	437	0.09	28.76	− 27.50	
#1759.43	46.98	6.72	1.87	3.59	3.79	37.64	560	438	0.09	41.43	− 28.59	
#1759.46	45.81	7.09	2.12	3.34	3.75	41.08	579	438	0.08	44.83	− 28.57	
#1759.85	46.86	7.21	2.59	2.79	4.39	42.68	592	437	0.09	47.07	− 28.26	
#1760.02	54.34	6.12	2.05	2.99	4.02	35.90	586	437	0.10	39.92	− 28.72	
#1760.38	41.24	7.39	4.31	1.71	3.85	44.33	600	439	0.08	48.18	− 27.76	
#1760.60	55.25	8.61	2.78	3.10	5.50	50.88	591	437	0.10	56.38	− 27.49	
#1760.80	52.23	8.46	2.62	3.23	5.24	51.16	605	436	0.09	56.40	− 27.26	
#1760.99	49.86	8.95	2.59	3.45	5.22	50.01	559	438	0.09	55.23	− 27.61	
#1761.06	38.80	2.73	1.82	1.50	1.94	13.60	499	435	0.12	15.54	− 27.55	
#1761.10	36.76	2.70	1.50	1.80	1.90	12.28	455	438	0.13	14.18	− 27.18	
#1761.16	80.15	2.96	0.60	4.96	3.13	18.16	614	436	0.15	21.28	− 26.61	
#1761.23	87.25	0.91	1.83	0.50	0.76	4.29	471	433	0.15	5.05	*n.d*	
#1761.30	56.76	4.48	1.87	2.40	3.91	28.26	630	437	0.12	32.17	− 26.85	
#1761.42	32.20	3.90	1.68	2.33	1.93	20.93	536	435	0.08	22.86	− 26.96	

Table 1 (continued)

| Sample ID (m)	Calcite (wt%)	TOC (wt%)	Sulphur (wt%)	TOC/S (–)	S_1 (mg HC/g rock)	S_2 (mg HC/g rock)	HI (mg HC/g TOC)	T_{max} (°C)	PI (–)	GP (mg HC/g rock)	$\delta^{13}C_{org}$ (VPDB; ‰)	
#1761.55	38.57	5.68	3.95	1.44	2.99	33.74	594	436	0.08	36.73	− 29.88	T-CIE
#1761.70	37.49	7.28	3.10	2.35	3.12	43.73	601	435	0.07	46.85	− 28.54	
#1761.71	36.19	7.44	2.70	2.75	3.13	47.19	634	437	0.06	50.32	− 30.94	
#1761.76	29.74	6.05	3.15	1.92	2.20	37.80	625	435	0.06	40.00	− 31.29	
#1761.79	46.54	6.59	2.41	2.74	3.23	41.84	634	435	0.07	45.07	− 31.33	
#1761.83	86.42	1.62	0.94	1.72	1.32	9.10	562	431	0.13	10.42	n.d	
#1761.88	21.29	4.81	3.76	1.28	2.04	27.58	574	434	0.07	29.62	− 32.05	
#1761.93	22.38	5.61	4.26	1.32	2.58	32.38	577	434	0.07	34.95	− 31.82	
#1762.00	20.10	6.53	4.50	1.45	2.60	36.94	565	436	0.07	39.53	− 31.14	
#1762.03	16.92	4.78	4.22	1.13	1.65	25.72	538	435	0.06	27.37	− 31.30	
#1762.08	14.46	4.95	3.33	1.49	1.74	28.64	579	435	0.06	30.37	− 33.05	
#1762.13	14.81	5.98	3.10	1.93	2.10	36.58	612	437	0.05	38.68	− 31.45	
#1762.19	17.28	5.74	2.89	1.99	2.02	33.02	575	433	0.06	35.03	− 31.39	
#1762.31	22.51	3.68	2.45	1.50	1.36	17.33	470	435	0.07	18.69	− 28.49	Pre-CIE
#1762.36	23.07	1.21	1.69	0.72	0.46	2.95	244	436	0.13	3.41	− 27.49	
#1762.43	21.90	2.85	1.63	1.75	0.90	11.56	405	438	0.07	12.46	− 27.78	
#1762.70	34.87	0.55	0.91	0.61	0.12	0.68	123	434	0.15	0.80	− 26.74	
#1762.86	31.13	1.84	2.00	0.92	0.48	6.60	358	435	0.07	7.08	− 28.06	
#1763.00	36.10	0.37	1.79	0.21	0.07	0.34	92	431	0.17	0.41	− 25.85	
#1763.06	34.61	2.68	1.33	2.02	0.84	11.35	423	435	0.07	12.19	− 28.48	
#1763.27	41.68	0.28	3.39	0.08	0.03	0.18	64	430	0.14	0.21	− 26.34	
#1763.44	44.14	0.26	0.56	0.46	0.04	0.17	66	430	0.17	0.21	− 25.74	
#1763.55	43.67	0.27	1.02	0.26	0.04	0.16	60	426	0.20	0.20	− 26.73	
#1763.63	86.44	0.12	0.08	1.54	0.06	0.06	49	426	0.50	0.12	n.d	
#1763.75	51.00	0.15	0.23	0.65	0.11	0.26	173	428	0.28	0.37	n.d	
#1763.83	87.25	0.09	0.08	1.13	0.01	0.03	33	424	0.25	0.04	n.d	
#1763.85	86.51	0.11	0.08	1.29	0.06	0.08	71	426	0.44	0.14	n.d	
#1763.98	49.67	0.15	1.12	0.13	0.03	0.12	80	428	0.20	0.15	− 26.35	
#1764.10	54.89	0.26	0.53	0.48	0.02	0.14	55	430	0.13	0.16	− 27.07	
#1764.65	58.58	0.24	0.82	0.30	0.06	0.17	70	428	0.26	0.23	− 26.73	
#1764.90	61.22	0.26	0.51	0.50	0.02	0.14	54	430	0.13	0.16	− 26.16	

GP generation potential
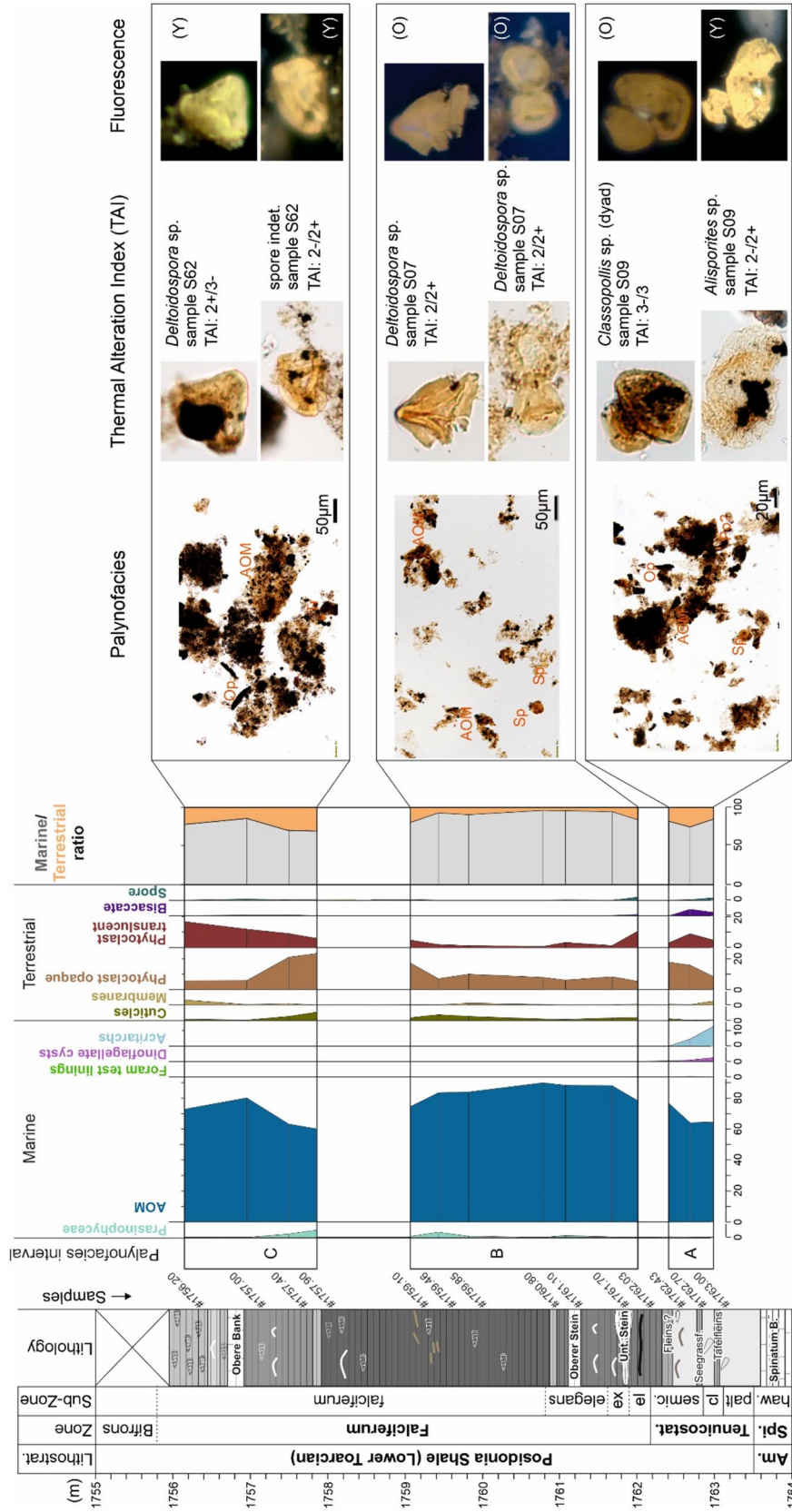
Fig. 4 Particulate organic matter and photomicrographs of the organic matter component, thermal alteration index (TAI) and fluorescence colour. *AOM* amorphous organic matter, *TR* translucent phytoclasts, *Op* opaque phytoclasts, *Sp* spore, *Po* pollen grain

Springer

International Journal of Earth Sciences

Table 2 Palynofacies percentages (in vol%) for Toarcian sediments from the Salem drill core

Sample ID [m]	Marine					Terrigenous						Σ MOM	Σ TOM
	AOM	Acritarchs	Dinoflagel-late cysts	Prasino-phytes	Foraminiferal test linings	Phytoclasts translucent	Phyto-clasts opaque	Cuticles	Membranes	Bisaccate	Spore		
Post_CIE													
#1756.20	72.82	0.00	0.00	0.20	0.00	16.87	5.75	0.99	3.37	0.00	0.00	73.02	26.98
#1757.00	80.20	0.00	0.00	0.00	0.00	11.96	5.88	0.39	0.39	0.39	0.78	80.20	19.80
#1757.54	63.21	0.00	0.00	2.22	0.00	9.14	20.99	2.72	0.99	0.49	0.25	65.43	34.57
#1757.90	60.14	0.00	0.00	4.77	0.00	5.97	23.39	5.49	0.00	0.00	0.24	64.92	35.08
#1759.10	74.53	0.00	0.00	0.71	0.00	4.95	17.22	1.89	0.24	0.00	0.47	75.24	24.76
#1759.46	83.52	0.00	0.00	3.34	0.00	2.00	7.13	3.79	0.22	0.00	0.00	86.86	13.14
#1759.85	83.99	0.00	0.00	0.83	0.00	1.25	9.98	2.70	1.25	0.00	0.00	84.82	15.18
#1760.80	89.93	0.00	0.00	0.00	0.00	0.71	7.95	1.06	0.35	0.00	0.00	89.93	10.07
#1761.10	88.35	0.00	0.00	1.17	0.00	3.30	6.21	0.78	0.00	0.00	0.19	89.51	10.49
T-CIE													
#1761.70	88.06	0.00	0.00	0.29	0.00	1.29	8.35	1.73	0.14	0.14	0.00	88.35	11.65
#1762.03	78.31	0.00	0.00	0.00	0.20	10.64	5.42	2.01	0.60	0.80	2.01	78.51	21.49
Pre-CIE													
#1762.43	76.49	0.00	0.40	0.40	0.00	3.19	17.73	1.20	0.60	0.00	0.00	77.29	22.71
#1762.70	64.18	4.48	0.90	0.30	0.30	8.96	15.82	0.30	0.30	4.18	0.30	70.15	29.85
#1763.00	64.59	12.68	2.41	0.00	0.00	4.83	8.45	0.60	2.62	2.21	1.61	79.68	20.32

AOM amorphous organic matter, *MOM* marine organic matter, *TOM* terrigenous organic matter, *Σ* sum
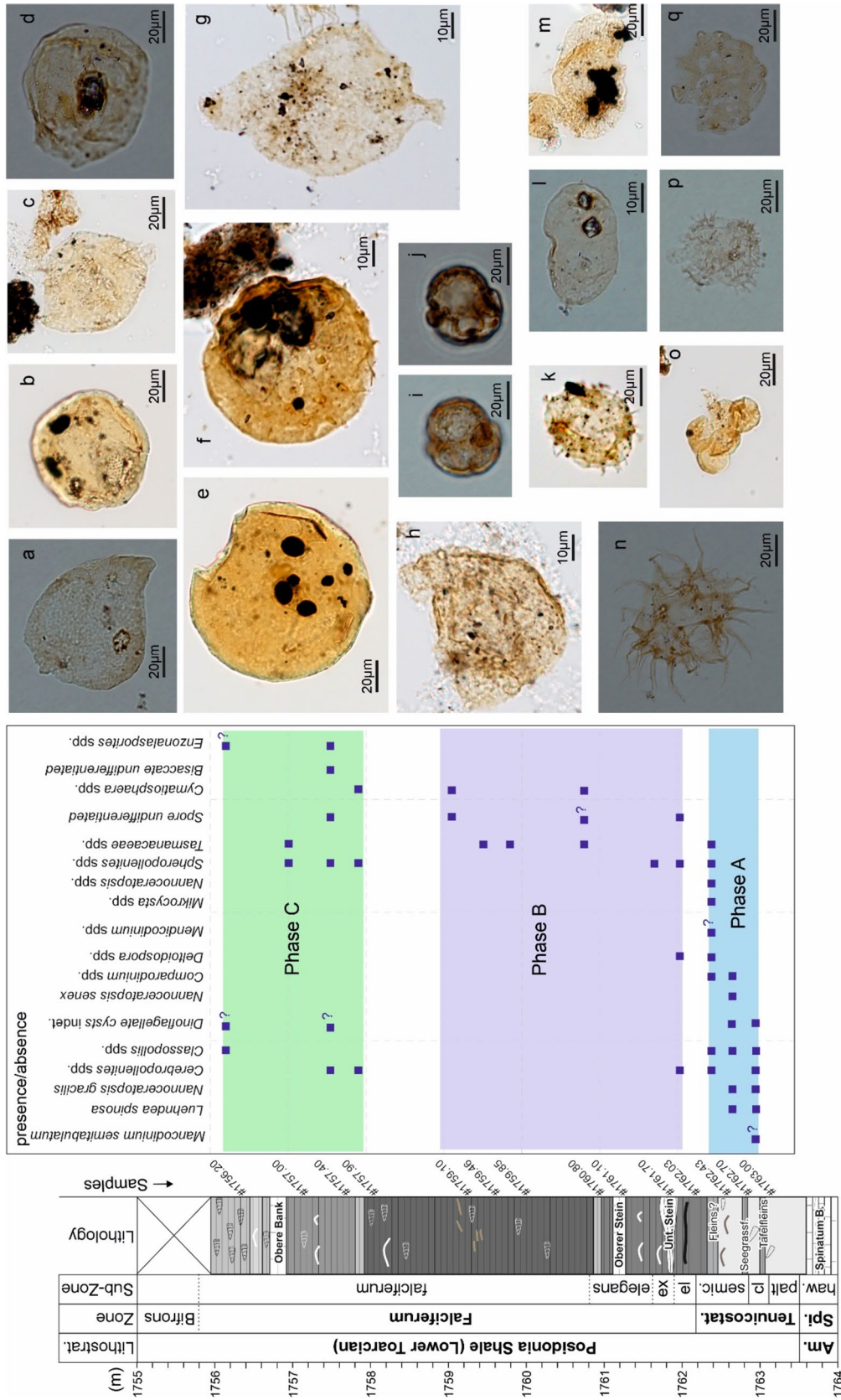
Fig. 5 Presence/absence data of terrestrial and marine palynomorphs. Each blue square represents a minimum of two occurrences of the respective dinoflagellate cyst and sporomorph. Characteristic assemblage from lower Toarcian strata of Salem core (SW Germany). The sample number is followed by the specification of the slide (**K**=kerogen **O**=oxidized), and England Finder coordinates. **a** *Nannoceratopsis gracilis*, #1763.00 **O**, O9. **b** *Cymathiosphaera* sp., #1763.00 **O**, X37/2. **c** *Nannoceratopsis senex*, #1759.10K, U59. **c** *Nannoceratopsis senex*, #1763.00 **O**, O38/1. **d** Dinoflagellate cyst indet., #1763.00 **O**, X37/2. **e** *Tasmanites* sp., #1760.80K, D63/4. **f** *Pterosphaeridia* sp., #1762.70K, P67/1. **g** *Nannoceratopsis senex*, #1763.00K, V47/2. **h** *Mancodinium semitabulatum*, #1762.70K, S57/2. **i** *Mikrocysta* sp., (high focus). #1763.43 **O**, V44/3. **j** *Mikrocysta* sp., (low focus). #1763.43 **O**, V44/3. **k** *Mendicodinium spinosum perforatum*, #1763.43 **O**, Q67. **l** *Comparodinium punctatum*, #1763.00 **O**, O11/4. **m** *Alisporites robustus*, #1763.00K, Q54/1. **n** *Luehndea spinosa*, #1763.43 **O**, Z51/4. **p** *Mendicodinium* sp., #1763.43 **O**, O47/4. **o** *Spheripollenites* sp., #1762.03 **O**, R16/1. **o** *Spheripollenites* sp., #1762.03 **O**, Z51/4. **p** *Mendicodinium* sp., #1763.43 **O**, O47/4. **q** *Mancodinium* sp., #1763.00 **O**, S42/3

Table 3 Maceral percentages (in vol%) for Toarcian sediments from the drill core (Rr = Vitrinite reflectance, s = standard deviation, n = number of measurements)

Sample ID (m)	Vitrinite (vol%)	Inertinite (vol%)	Sporinite (vol%)	Telalginite (vol%)	Lamalginite (vol%)	Liptodetrinite (vol%)	Rr/s/n
Post-CIE							
#1756.20	10	8	8	0	64	10	
#1757.00	7	7	7	13	60	7	
#1757.90	9	3	3	20	60	5	
#1759.10	8	6	8	17	60	1	
#1759.85	6	6	11	6	67	6	
#1760.80	6	2	0	6	87	0	
#1760.99	3	16	0	24	16	42	
T-CIE							
#1761.70	4	7	0	14	75	0	
#1761.93	36	2	0	19	27	17	0.69/0.12/29
Pre-CIE							
#1762.70	5	8	0	31	55	0	
#1763.44	14	71	0	0	14	0	

opaque phytoclasts are recorded in similar relative abundances as in interval A (~ 10%). Interval B marks the onset of a major marine turnover from a dinoflagellate-cyst- to prasinophytes-dominated assemblage (Fig. 4, Table 2).

Interval C occurs in the samples from the upper part of the core (#1757.90 to #1756.20). Although a high percentage of AOM is still present (~ 65%), the terrestrial fraction rapidly increases again. While sporomorphs are fairly common and prasinophytes are frequent, dinoflagellate cysts are unrecovered.

As shown in Fig. 4, spore colour ranges from a TAI value of 3−/3 at the bottom of the borehole to values of 2+/3− at the top of the studied core falling within the mature stage of hydrocarbon generation (Taylor et al. 1998; Yule et al. 1998).

Palynology

The Salem samples yielded few palynomorphs. The preservation is extremely variable, with palynomorphs reasonably well preserved in the lower part of the borehole, and poorly preserved in the rest of it. Thus, in some cases, sporomorphs were not assignable to any taxon. Consequently, the analysis of the relative abundances of palynomorphs and dinoflagellate cysts was impossible. The occurrence data are displayed in Fig. 5. Each dot represents a minimum of two occurrences for dinoflagellate cysts and sporomorphs.

In interval A, dinoflagellate cysts are highly common and diverse with *Luehndea spinosa, Nannoceratopsis* spp., *N. gracilis, N. senex,* and *Comparodinium punctatum.* The terrigenous fraction contains several pollen grains with *Classopollis* spp., *Alisporites* sp. and *Cerebropollenites* spp. The last occurrence datum (LOD) of *Luehndea spinosa* is

recorded in sample #1762.70 at the base of the thick black shale succession. A drastic reduction in dinoflagellate cysts taxonomic diversity occurs in sample S08, containing only a questionable *Mendicodinium spinosum perforatum* and *Mendicodinium* sp.

From sample #1762.03 (interval B) onward, a major floral turnover was recorded, from a dinoflagellate-cyst-dominated assemblage to one with an elevated amount of prasinophytes (e.g., *Spheripollenites* spp. and *Tasmanaceae* spp.). Pollen grains and spores are reduced. Interval C samples do not show dinoflagellate cysts, but an elevated number of *Spheripollenites* sp. and prasinophytes are still documented.

Maceral analysis

Liptinite is the dominating maceral group in most samples (> 80 vol%), while vitrinite and inertinite are typically much less abundant (Table 3; Fig. 6). Exceptions are the low-TOC (0.26%) sample #1763.44 and sample #1761.93 from the lower part of the T-CIE, which contain very high amounts of inertinite and vitrinite, respectively. Lamalginite and telalginite are present in all samples. Typically, lamalginite is significantly more abundant than telalginite (including tasmanite algae; Fig. 6). Vitrinite reflectance was determined for the vitrinite-rich sample #1761.93 (lower part of the T-CIE) and yielded a value of 0.69 ± 0.12%Rr. No correlation exists between the maceral groups and TOC, probably because some of the OM is present as sub-microscopic particles.

Molecular composition of hydrocarbons

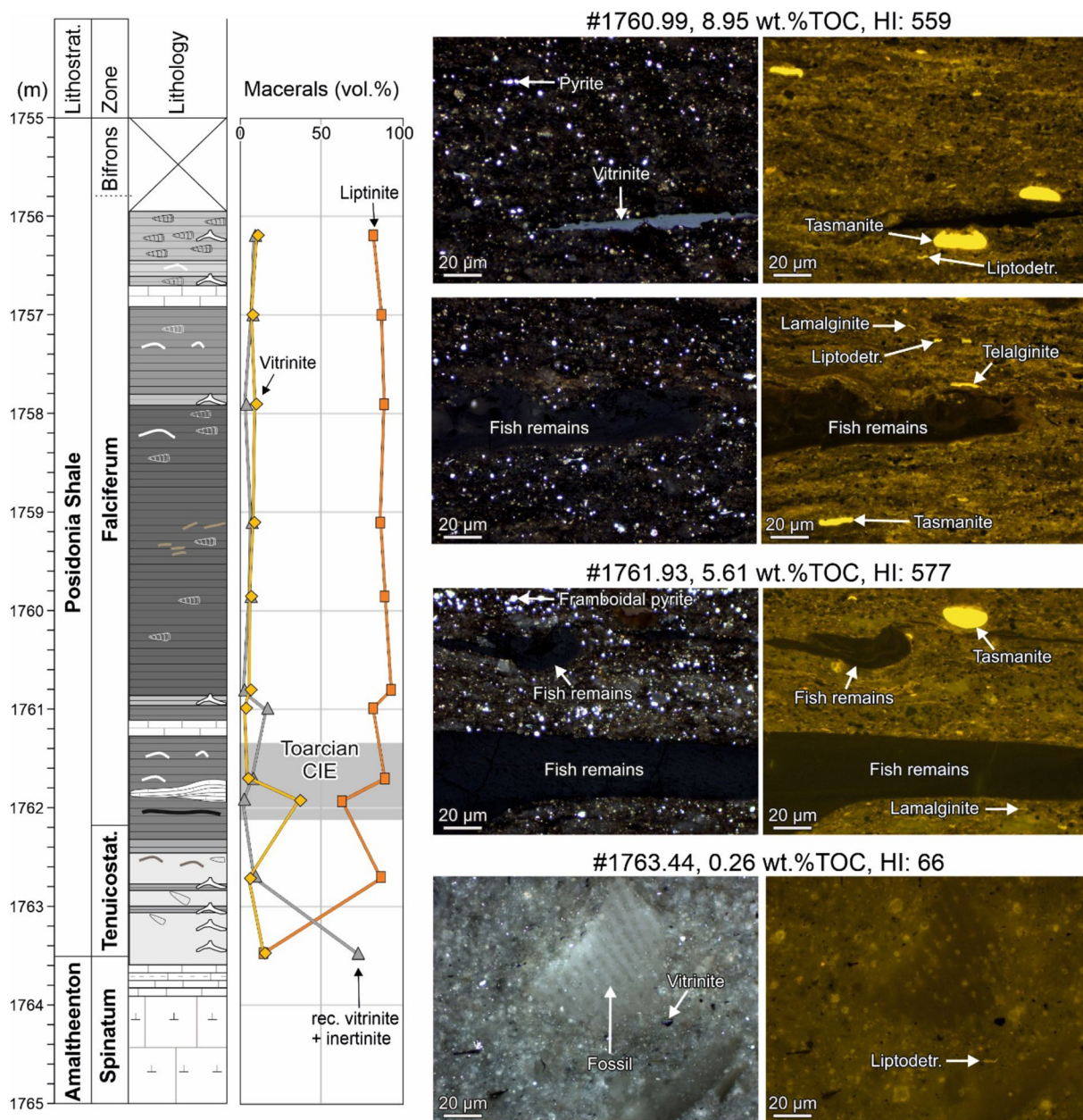Representative GC-FID and GC–MS traces for the 31 samples investigated for biomarkers are displayed in Figs. 7 and

Fig. 6 Maceral composition of Salem samples with micro-photomicrographs of selected samples (left: white light; right: fuorescence mode)

8. Concentrations and ratios of selected molecular compounds are presented in Table 4 and plotted versus depth in Fig. 9.

n-Alkanes and isoprenoids

The *n*-alkane patterns are characterised by a unimodal distribution with chain lengths ranging from *n*-C$_{15}$ to *n*-C$_{35}$. A clear distinction can be made between the distribution patterns of the Amaltheenton Formation and that of the Posidonia Shale (Fig. 7).

The *n*-alkanes concentrations vary between 716 and 7435 µg/g TOC. Their concentration ratios are dominated by short-chain *n*-alkanes (*n*-C$_{15-19}$/∑*n*-alkanes: 0.38–0.70) followed by mid- (*n*-C$_{21-25}$/∑*n*-alkanes: 0.12–0.29) and long-chain *n*-alkanes (*n*-C$_{27-31}$/∑*n*-alkanes: 0.05–0.15) (Fig. 9a). The highest amounts of short-chain *n*-alkanes occur in the Amaltheenton Formation with concentration ratios that decrease upward. The carbon preference index (CPI) values (according to Bray and Evans 1961) are close to unity within and above the T-CIE, whereas below this interval, the value

varies from 1.15 to 2.33. The highest CPI occurs within the underlying Amaltheenton Formation (Fig. 9b).

Isoprenoid concentrations vary from 167 to 1579 µg/g TOC. The pristane/phytane (Pr/Ph) ratio (Didyk et al. 1978) ranges from 0.72 to 2.54. It increases upwards from the Amaltheenton Formation (0.75–1.11) to the top of the Posidonia Shale below the T-CIE (2.31). Relatively low values (1.54–1.82) occur within the T-CIE, while values around 2.0 prevail in the sediments above the T-CIE. Even higher values (2.17–2.54) occur above 1758 m depth (Fig. 9c).

The $(Pr + Ph)/(n$-$C_{17} + n$-$C_{18})$ ratio reflects maturity and biodegradation. However, Frimmel et al. (2004) showed that in case of the Posidonia Shale in SW Germany it is also a useful redox parameter. It increases upwards from the Amaltheenton Formation (0.35–0.53) to the base of the T-CIE (~ 0.8) and shows high ratios (0.88–1.17) within the T-CIE interval. Above this interval the ratio decreases to 0.77 at 1758.55 m and is relatively low (0.35–0.77) in the interval above 1758 m depth (Fig. 9e; Table 4). For organic matter-rich samples (TOC > 1.0 wt%) there is a strong negative correlation between the Pr/Ph and (pristane + phytane)/ $(n$-$C_{17} + n$-$C_{18})$ ratios ($r^2 = 0.79$).

Steroids

Sterane concentrations are typically low (7–153 µg/g TOC). Very low concentrations occur in the Amaltheenton Formation, as well as in the lower- and uppermost parts of the Posidonia Shale (Table 4). Within the Posidonia Shale section, C_{27} steranes are typically, slightly more abundant than C_{29} steranes, while C_{28} steranes occur in low amounts. High concentrations of C_{28} steranes have been determined for only two low-TOC samples from the Amaltheenton Formation (#1764.1, #1764.9 m) and might be artefacts (Fig. 9f; Table 4).

The C_{29} sterane $20S/(20S + 20R)$ ratio and the C_{29} sterane $\alpha\beta\beta/(\alpha\beta\beta + \alpha\alpha\alpha)$ ratios are thermal maturity parameters (Seifert and Moldowan 1986). In organic matter-rich samples, C_{29} sterane $20S/(20S + 20R)$ ratios vary between 0.40 and 0.61 (0.51 on average) and the C_{29} sterane $\alpha\beta\beta/(\alpha\beta\beta + \alpha\alpha\alpha)$ ratios vary between 0.50 and 0.63 (0.57 on average). Both ratios show a subtle upward decrease. In contrast, organic-lean sediments from the Amaltheenton Formation and from the base of the Posidonia Shale, partly show significantly lower ratios (0.03–0.52 and 0.18–0.58) (Table 4). As data from organic-lean sediments might be biased by low extraction yields, they were not considered for interpretation.

The following 4-methylsteranes were identified in most of the samples: C_{28}: 4α-methyl-5α-cholestane, C_{29}: 4α, 24-dimethyl-5α-cholestane, C_{30}: 4α-methyl-24-ethyl-5α-cholestane, and dinosterane (4α, 23S,

24R-trimethyl-5α-cholestane) isomers (Figs. 9h–j, 10). Their highest concentrations are observed within the Posidonia Shale Formation above the "Unterer Stein" above which they begin to gradually decrease upwards. Below the "Unterer Stein", these concentrations are notably lower (Fig. 9h–j).

Hopanoids and related compounds

Hopanes dominate the non-aromatic cyclic triterpenoids with concentrations ranging from 10 to 290 µg/gTOC. The highest concentration occurs in the lower part of the T-CIE (Table 4).

The steranes/hopanes ratio varies strongly in organic-lean sediments (0.39–4.53). In the organic matter-rich part of the Posidonia Shale, the ratio increases upward from the base of the T-CIE (0.31), reaches a maximum of 1.16 within the sediments above the T-CIE at a depth of 1759.85 m and decreases again above this level (Fig. 9k).

There is a constant decrease in concentration from carbon number C_{31} to C_{35} 17α,21β(H)-homohopanes (Fig. 7). The C_{31} hopane isomerization ratios of $22S/(22S + 22R)$ are at equilibrium (~ 0.60; Mackenzie and Maxwell 1981), but lower values occur in some samples with very low TOC (Table 3).

The moretane/hopane ratios are between 0.18 and 0.38 in low-TOC samples and vary between 0.14 and 0.21 in the black shale part. A subtle increase can be observed above the T-CIE (Table 4). The $T_s/(T_s + T_m)$ ratios varies between 0.23 and 0.53 (Fig. 9m). The Gammacerane Index [GI = gammacerane/(gammacerane + C_{30} hopane)]; Sinninghe Damsté et al. 1995) ranges from 0.02 to 0.12 with maximum value occurring at 1759.1 m depth. Remarkably, GI is low (~ 0.02) within the T-CIE interval (Table 3).

Tricyclic terpanes (TT) concentrations are significant and range from 4 to 52 µg/g TOC. There is a very strong positive correlation between TTs and hopanes ($r \sim = 0.90$). Similar to hopanes, the highest TT concentrations occur within the T-CIE interval (Fig. 9o; Table 3). The TTs occur within their C_{19} to C_{29} chain length. C_{23} TT is the most prominent one, followed by C_{19}, C_{20}, and C_{21}, while C_{27} is absent (Fig. 7). Depth plots of C_{19}/C_{23} TT, C_{20}/C_{23} TT show that the low-TOC samples below the T-CIE have higher C_{19}/C_{23} TT, C_{20}/C_{23} TT ratios than the black shales (Fig. 9n; Table 4). Amongst the latter, relatively high ratios occur in the uppermost part of the studied section (1758–1756 m).

Aromatic hydrocarbons

The aromatic fraction of the Posidonia Shale and the Amaltheenton Formation contain low to significant amount of benzenes, napthalenes, phenanthrenes,
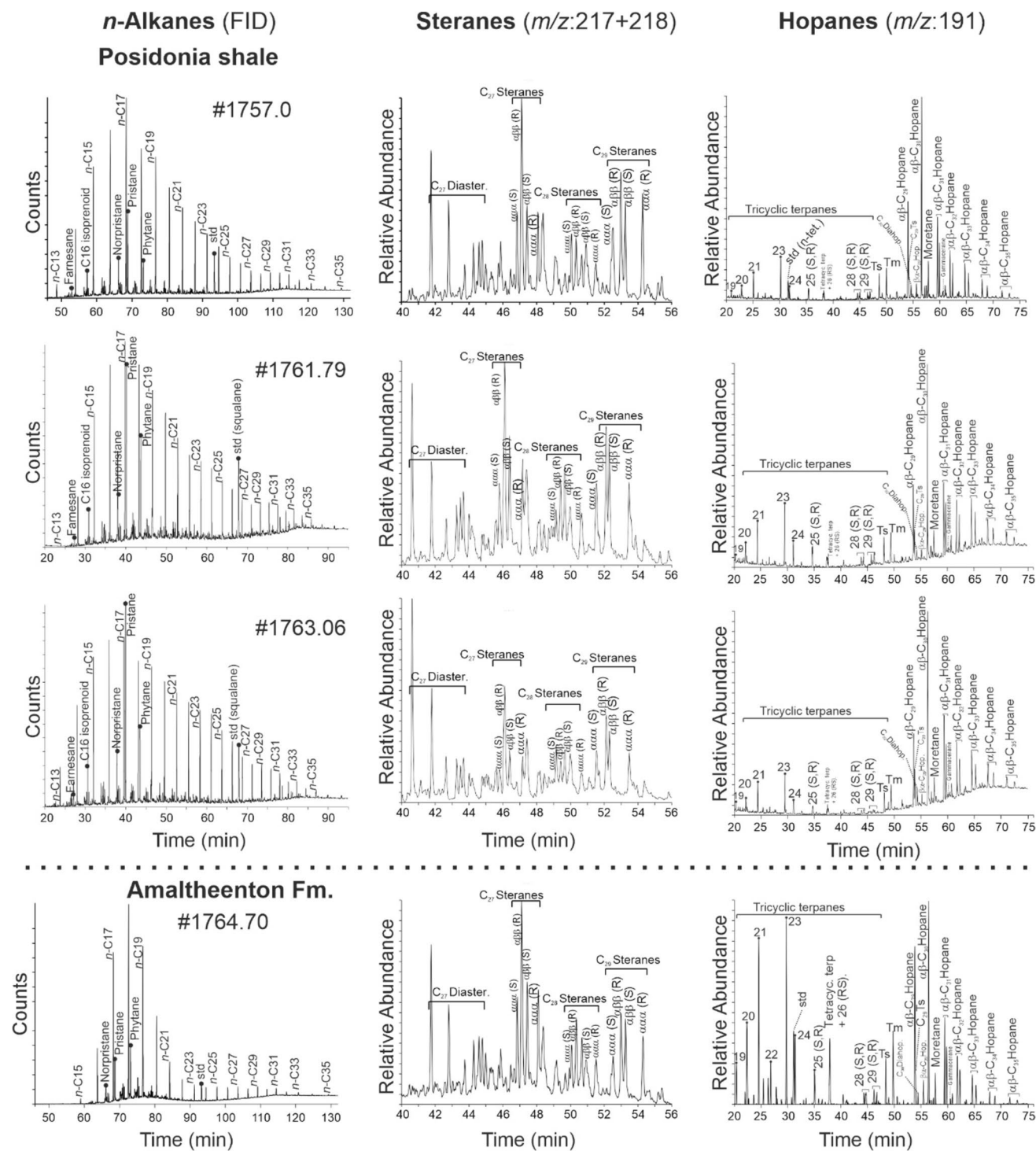
Fig. 7 Flame ionization detector (FID) traces of the saturated hydrocarbon fraction and mass chromatogram representations of steranes, tricyclic terpanes and hopanes of samples from different stratigraphic positions within the Salem well. Std-deuterated n-tetracosane, $C_{24}D_{50}$

dibenzothiophenes, and their alkylated analogues (Table 3; Fig. 8). Relevant alkylphenanthrenes present include methylphenanthrenes (MP), and dimethylphenanthrene (DMP)

with concentrations varying from 31–156 and 51–306 µg/g TOC, respectively. The methylphenanthrene index (MPI-1; Radke et al. 1986; Radke 1988) in black shales varies from 0.38 to 0.53 (0.46 on average), while it is slightly higher
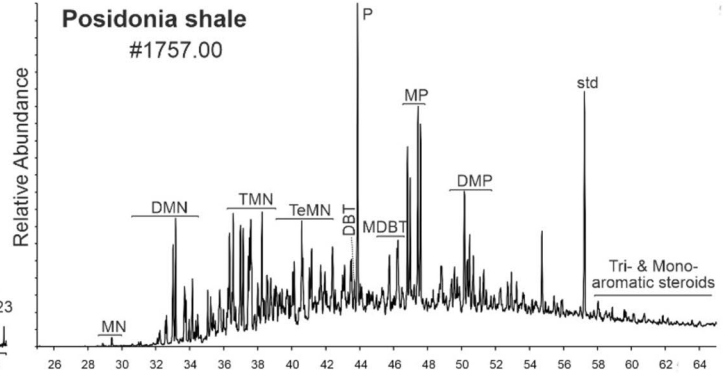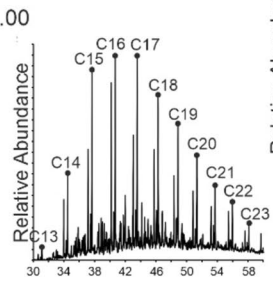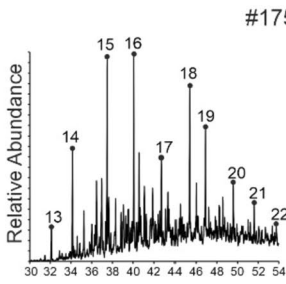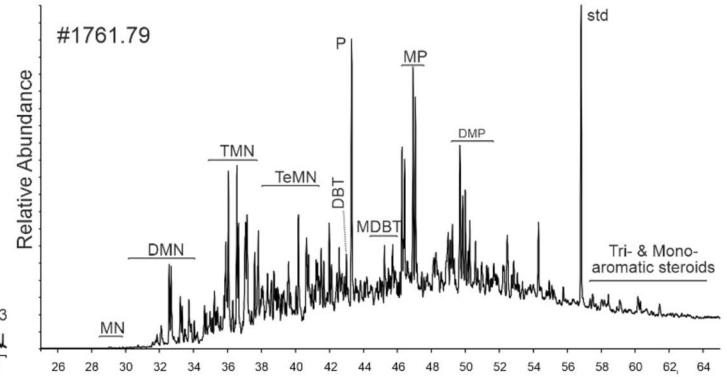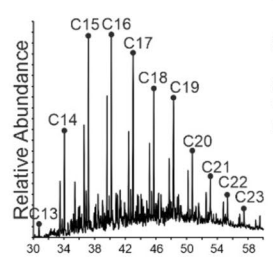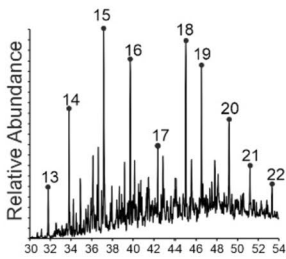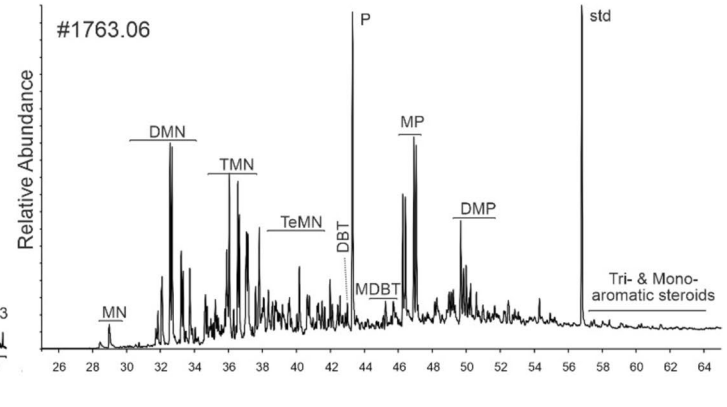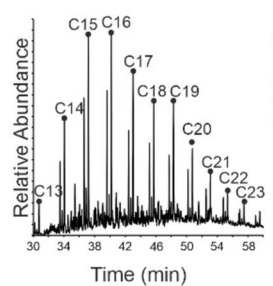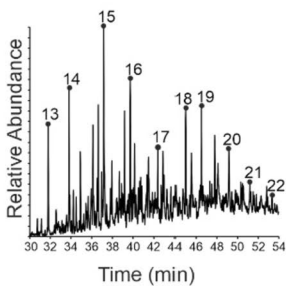
◀ **Fig. 8** Mass chromatogram representations of arylisoprenoids, methyl-*n*-alkybenzenes (number given in chromatogram represents a t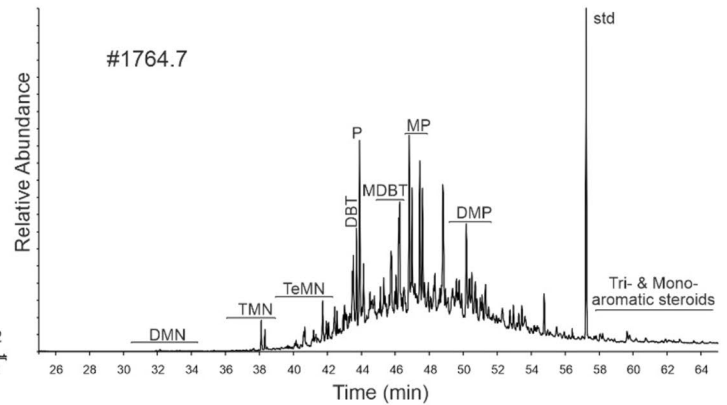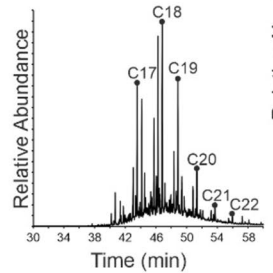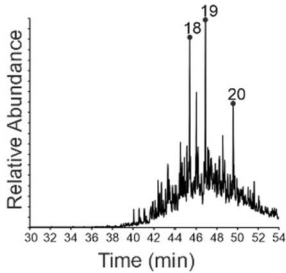otal number of C-atoms in arylisoprenoids and methyl-*n*-alkylbenzenes) naphthalenes, dibenzothiophenes, phenanthrenes and aromatic steroids of samples from different stratigraphic positions within the Salem well. Std-1,1′-binaphthyl

in organic-lean sediments (0.49–0.65; 0.55 on average). The average equivalent vitrinite reflectance derived from the MPI-1 is 0.68%Rr for black shales and 0.73%Rr for organic-lean deposits (Table 4). Concentrations of methyldibenzothiophenes (MDBT) are low (3–33 µg/g TOC). The methydibenzothiophene ratio (MDR; Radke et al. 1986) ranges from 1.17 to 2.19. The dibenzothiophene/phenathrene (DBT/Phen) ratios are generally low (0.06–0.17) and show the highest value in the upper part of the T-CIE (Fig. 9p). Mono- (0.2–7.4 µg/g TOC) and tri- (0.4–18 µg/g TOC) aromatic steroids are present in low concentrations. Significant concentrations of methyl-*n*-alkylbenzenes are present in the aromatic fraction (Table 4) ranging from 51 to 558 µg/g TOC and reaching the maximum just above the T-CIE (Fig. 9q).

Aryl isoprenoids with C_{13} to C_{23} chain distribution are present with low to moderate concentrations (7–121 µg/g TOC). Their concentrations are low below the T-CIE, increase upwards within the T-CIE, reach a maximum immediately above the T-CIE and decrease gradually in the upper part of the section (Fig. 9r). The arylisoprenoid ratio (AIR = C_{13-17}/C_{18-22} aryl isoprenoids; Schwark and Frimmel 2004) ranges from 0.09 to 1.92. Within the Posidonia Shale, AIR increases upwards, but is relatively low in the uppermost samples (Fig. 9r).

Stable carbon isotope composition of selected organic molecules

Compound-specific carbon isotope ratios were determined for a sub-set of the samples. Carbon isotope ratios are presented for *n*-alkanes with 15–29 carbon atoms and for selected isoprenoids (norpristane, pristane, and phytane) in Table 5. All studied *n*-alkanes show a negative shift of $\delta^{13}C$ ratios in the T-CIE interval (Fig. 11) with the most negative values in the interval below the "Unterer Stein". The negative shift of $\delta^{13}C$ ratios is slightly higher for mid- and long-chain *n*-alkanes (3.5–4.0‰) than for short-chain *n*-alkanes (~3‰). The strongest negative shift in $\delta^{13}C$ for all *n*-alkanes is recorded for sample #1762.13.

$\delta^{13}C$ ratios of pristane are slightly more negative than those of phytane, but both compounds show only a moderate negative shift in the T-CIE (~2‰; Fig. 11) and are in the range of $\delta^{13}C$ ratios of those from the Seegrasschiefer and the Tafelfleins. In contrast to *n*-alkanes, $\delta^{13}C$ ratios of pristane and phytane are uniform within the T-CIE and return to background values only at 1761.30 m depth.

The variation of $\delta^{13}C$ values, as a function of chain length of *n*-alkanes, is shown in Fig. 12 together with $\delta^{13}C$ values of norpristane, pristane and phytane. Low-TOC samples from the Amaltheenton Formation (#1764.90 to #1763.55) are characterised by high $\delta^{13}C$ ratios and an increase in $\delta^{13}C$ with increasing chain length. Pristane and phytane show similar $\delta^{13}C$ values than short-chain *n*-alkanes. Low- and high-TOC samples from the Posidonia Shale below the T-CIE (#1763.06 to #1762.31) are isotopically lighter and *n*-alkanes with different chain lengths show fairly uniform $\delta^{13}C$ values, but short-chain *n*-alkanes from the organic matter-rich "Fleins" (#1762.31) are characterised by low $\delta^{13}C$ values. $\delta^{13}C$ values of isoprenoids are in the range of those for *n*-alkanes.

Samples from the lower part of the T-CIE interval (#1762.13 to #1761.93) are isotopically lighter than the rest of the samples. They show decreasing $\delta^{13}C$ values with increasing chain length for short- and mid-chain length *n*-alkanes and constant values for long-chain *n*-alkanes. $\delta^{13}C$ values of isoprenoids from these samples are higher than for *n*-alkanes. In contrast, samples from the uppermost part of the T-CIE (#1761.79, #1761.70) are isotopically slightly heavier and show uniform $\delta^{13}C$ values for *n*-alkanes with varying carbon numbers. $\delta^{13}C$ values of pristane and phytane from these shallow samples are similar to those of the *n*-alkanes.

CSI data from samples above the T-CIE are rather uniform. *n*-C_{15} and *n*-C_{16} in all samples are isotopically relatively heavy, while *n*-alkanes with longer chain length show similar $\delta^{13}C$ values between −31 and −33‰. $\delta^{13}C$ values of pristane and phytane are similar to those of *n*-alkanes.

Discussion

Thermal maturity

Thermal maturity parameters such as vitrinite reflectance (0.69 ± 0.12%Rr), T_{max} (436 °C on average) and TAI (2–3) suggest that the Posidonia Shale at Salem has reached early to peak oil window maturity. The average equivalent vitrinite reflectance derived from the MPI-1 is 0.68%Rr for black shales and 0.73%Rr for organic-lean deposits. Oil window maturity is also supported by 20S/(20S + 20R) and $\alpha\beta\beta/(\alpha\beta\beta + \alpha\alpha\alpha)$ C_{29} sterane isomerisation ratios (0.51 and 0.57 on average, respectively; Fig. 13) and by the 22S/(22S + 22R) C_{31} hopane ratio (0.60 on average; Mackenzie and Maxwell 1981).

Maturity parameters from immature to early oil window mature Dormettingen samples (0.40–0.54%Rr; Ajuaba et al. 2022) are plotted in Fig. 13a for comparison. PI of black shales at Salem is higher than at Dormettingen (0.08 and 0.04 on average, respectively), but still below the value of

0.10, which is often taken as the threshold value for the onset of the oil window (e.g., Peters 1986; Fig. 13b). Evaporative loss of S1 is considered unlikely but cannot be excluded as the core was taken about 50 years ago. In any case, the value indicates that some hydrocarbons have already been generated. This fact must be taken into account when discussing the (remaining) hydrocarbon potential and evaluating environmental proxies based on organic geochemical data.

Source rock potential

High TOC contents (average 4.9 wt%) and high HI values (~530 mgHC/gTOC) show that the Posidonia Shale at Salem has an excellent hydrocarbon generation potential. The high source rock potential of the Posidonia Shale in the SWGB has been shown previously by Littke et al. (1991b). Indeed, the Posidonia Shale has been assumed by many authors (e.g., Wehner and Kuckelkorn 1995; Veron 2005; Misch et al. 2017) to be one of the main source rocks in the North Alpine Foreland Basin, although Bechtel et al. (2019) showed that it contributed only to oil deposits west of Munich.

Interestingly, the average HI at Salem is significantly lower than at Dormettingen (~650 mgHC/gTOC; Ajuaba et al. 2022). Although a facies effect on HI cannot be excluded, this difference may suggest that 15–20% of the original hydrocarbon potential has already been generated at Salem. This percentage is even higher, if the possible presence of retained bitumen, which forms part of the S_2 peak (e.g., Ziegs et al. 2017), is assumed.

The Source Potential Index {SPI (tHC/m^2) = [$S_1 + S_2$ (mgHC/g rock)] × thickness (m) × rock density (g/cm^3)/1000} of Demaison and Huizinga (1994), which gives the amount of hydrocarbon generated beneath one square meter of surface area, is used to quantify the remaining source rock potential of the Posidonia Shale at Salem.

For the calculation, an average rock density of 2.55 g/cm^3 (cf. Stock and Littke 2018) has been used. Following the guidelines of Demaison and Huizinga (1994), low-TOC layers were not used for the calculation of the average genetic potential ($S_1 + S_2$: 31.5 mgHC/g rock) and the net source rock thickness (6.43 m). On that assumption, the SPI for the cored interval is calculated as 0.49 tHC/m^2 (Table 6). For comparison, the SPI has been calculated for the same stratigraphic interval (Posidonia Shale below the "Inoceramen Bank") using data from the Dormettingen section (Ajuaba et al. 2022). The comparison shows a slightly higher SPI for Dormettingen (0.58 tHC/m^2; Table 6). The difference is mainly due to the significantly higher genetic potential at Dormettingen (52.10 mgHC/g rock), which overcompensates for it being less thick.

The SPI of the upper part of the Posidonia Shale at Dormettingen (*bifrons* Zone) is 0.53 tHC/m^2. No data is available from that interval from Salem. However, considering it is less thick (3 versus 4 m) and has a lower genetic potential, the SPI might be in the order of 0.30 tHC/m^2 suggesting a total SPI of 0.80 tHC/m^2.

Littke et al. (1991b) presented average HI and PI data for Posidonia Shale in four boreholes located along the Swabian Alb between Aselfingen and Stuttgart (see Fig. 1b). Using these data, the average genetic potential ($S_1 + S_2$) and the SPI have been determined for these wells (Table 6). These SPI values for the entire Posidonia Shale (0.56–0.98 tHC/m^2) are in the same order of magnitude than those for Salem and Dormettingen. This implies that the Posidonia Shale has a slightly lower SPI than the entire Lower Oligocene in the Austrian part of the North Alpine Foreland Basin (1.09 tHC/m^2), but a higher SPI than the main source rock interval (Schöneck Formation) alone (0.35 tHC/m^2; Sachsenhofer et al. 2010).

The Posidonia Shale is also an important source rock in the Northwest German Basin (e.g., Bruns et al. 2013; Stock and Littke 2018). Using Rock–Eval data from the Wickensen well, where the Posidonia Shale is about 30 m thick and the organic matter is thermally immature (Littke et al. 1991a; Burnaz et al. 2024), a SPI of 5.8 tHC/m^2 is calculated (Table 6). This shows that not only the petroleum potential of the Posidonia Shale in northwest Germany is significantly higher than in the SWGB, which is a result of greater thickness, but also a higher genetic potential ($S_1 + S_2$; cf. Table 6), which is also reflected in a significantly higher average HI (720 mgHC/gTOC; Burnaz et al. 2024).

Depositional environment

Geochemical and palynological proxies are employed in this section to reconstruct the depositional environment of the Posidonia Shale at Salem. In this regard, extensive published information on the Posidonia Shale in SW Germany, especially on the Dotternhausen/Dormettingen sections, is taken into account (Röhl et al. 2001; Schmid-Röhl et al 2002; Frimmel et al. 2004; Schwark and Frimmel 2004; Röhl and Schmid-Röhl 2005; van den Schootbrugge et al. 2005; Bour et al. 2007; van Acken et al. 2019; Wang et al. 2020, 2021; Galasso et al. 2021, 2022; Ajuaba et al. 2022).

Before the depositional environment is described for different stratigraphic units, some peculiarities of isoprenoid-based redox parameters are discussed. It is widely accepted that Pr/Ph ratios < 1 indicate anoxic conditions (e.g., Didyk et al. 1978). Although the Pr/Ph ratio is a reliable redox parameter for the Posidonia Shale, absolute values are skewed towards higher ratios (e.g., Schouten et al. 2000; Frimmel et al. 2004; Ajuaba et al. 2022). For example, Frimmel et al. (2004) showed that the limit for anoxic conditions in the case of Posidonia Shale is as high as 1.6. These authors also showed that the (Pr+Ph)/(n-C$_{17}$+n-C$_{18}$) ratio

Table 4 Concentrations and concentration ratios of compounds and compound groups within the hydrocarbon fractions of the Toarcian and Pliensbachian-samples of the Salem core

Sample ID [m]	n-alkanes						Steranes [µg/g TOC]	C27-29 steranes			20[S/(S+R)] C29 Steranes	αββ/(αββ + αααα) C29 Steranes	a	b	Methylsteranes [µg/g TOC]					Dinosteranes
	n-C15-19/	n-C21-25/	n-C27-31/	CPI	Pr/Ph	(Pr+Ph)/(n-C17+18)		C27/	C28/	C29/					C28-dia	C28	C29-dia	C29-	C30	
#1756.20	0.50	0.26	0.08	1.09	2.32	0.57	11	0.42	0.21	0.37	0.50	0.50	0.36	0.22	0.22	0.24	0.17	0.11	0.28	0.00
#1756.60	0.38	0.24	0.16	1.06	2.20	0.70	43	0.39	0.18	0.43	0.46	0.55	0.53	0.32	0.51	0.67	0.46	0.25	0.61	0.01
#1757.00	0.57	0.20	0.06	1.02	2.50	0.41	18	0.38	0.23	0.39	0.50	0.50	0.32	0.19	0.23	0.31	0.20	0.11	0.28	0.00
#1757.54	0.59	0.22	0.07	1.09	2.54	0.35	34	0.40	0.19	0.41	0.40	0.55	0.51	0.31	0.38	0.52	0.31	0.23	0.49	0.00
#1757.90	0.45	0.24	0.11	1.03	2.17	0.62	27	0.39	0.24	0.37	0.52	0.55	0.33	0.20	0.69	0.94	0.59	0.46	0.80	0.01
#1758.55	0.42	0.23	0.15	1.05	2.04	0.77	108	0.39	0.20	0.41	0.44	0.58	0.49	0.30	0.57	0.84	0.45	0.32	0.65	0.00
#1759.10	0.50	0.20	0.08	1.00	2.01	0.76	27	0.41	0.25	0.34	0.52	0.57	0.39	0.23	1.10	1.55	1.04	0.63	1.25	0.01
#1759.46	0.49	0.21	0.13	1.03	1.91	0.81	111	0.40	0.20	0.40	0.43	0.59	0.48	0.29	0.49	0.73	0.43	0.30	0.58	0.00
#1759.85	0.49	0.22	0.09	1.00	1.95	0.82	20	0.42	0.24	0.34	0.53	0.57	0.37	0.22	0.79	1.13	0.70	0.48	0.86	0.01
#1760.38	0.49	0.22	0.13	1.05	1.97	0.85	90	0.40	0.20	0.40	0.45	0.58	0.47	0.28	0.53	0.77	0.44	0.32	0.59	0.01
#1760.80	0.51	0.19	0.08	1.02	1.96	0.76	30	0.40	0.25	0.35	0.51	0.56	0.35	0.21	1.12	1.67	0.95	0.69	1.29	0.02
#1761.10	0.43	0.25	0.14	1.03	1.96	0.81	90	0.42	0.21	0.37	0.49	0.58	0.50	0.30	0.50	0.79	0.41	0.30	0.53	0.01
#1761.30	0.47	0.25	0.09	1.03	2.00	0.63	153	0.39	0.21	0.40	0.55	0.54	0.41	0.24	n.d	n.d	n.d	n.d	n.d	n.d
#1761.42	0.43	0.22	0.14	1.06	1.67	1.21	115	0.37	0.17	0.46	0.49	0.63	0.61	0.36	n.d	n.d	n.d	n.d	n.d	n.d
#1761.70	0.60	0.15	0.05	1.04	1.82	0.88	28	0.38	0.24	0.37	0.57	0.56	0.34	0.20	0.91	1.57	0.70	0.60	1.15	0.02
#1761.79	0.47	0.24	0.11	1.05	1.68	1.17	71	0.42	0.20	0.38	0.56	0.57	0.45	0.28	n.d	n.d	n.d	n.d	n.d	n.d
#1761.93	0.58	0.18	0.08	1.02	1.59	0.90	81	0.41	0.20	0.39	0.57	0.57	0.44	0.27	n.d	n.d	n.d	n.d	n.d	n.d
#1762.00	0.59	0.17	0.07	1.07	1.67	0.94	66	0.42	0.19	0.39	0.55	0.57	0.57	0.35	n.d	n.d	n.d	n.d	n.d	n.d
#1762.03	0.58	0.18	0.10	1.04	1.76	1.00	44	0.41	0.20	0.38	0.46	0.57	0.53	0.32	0.31	0.45	0.26	0.16	0.34	0.00
#1762.08	0.57	0.18	0.08	1.08	1.62	1.00	99	0.39	0.21	0.39	0.53	0.55	0.50	0.30	n.d	n.d	n.d	n.d	n.d	n.d
#1762.13	0.54	0.21	0.09	1.05	1.54	1.13	72	0.39	0.21	0.40	0.58	0.57	0.49	0.29	n.d	n.d	n.d	n.d	n.d	n.d
#1762.31	0.41	0.29	0.12	1.09	2.18	0.79	51	0.35	0.23	0.42	0.61	0.61	0.82	0.49	n.d	n.d	n.d	n.d	n.d	n.d
#1762.70	0.47	0.27	0.10	1.15	1.33	0.42	12	0.45	0.21	0.33	0.52	0.53	0.34	0.38	0.14	0.17	0.09	0.07	0.15	0.00
#1762.86	0.46	0.25	0.11	1.09	2.29	1.13	43	0.34	0.19	0.47	0.49	0.56	0.42	0.21	n.d	n.d	n.d	n.d	n.d	n.d
#1763.00	0.50	0.23	0.11	1.29	1.64	0.59	11	0.45	0.18	0.37	0.33	0.43	0.46	0.42	0.06	0.07	0.04	0.03	0.07	0.00
#1763.06	0.40	0.27	0.11	1.07	2.69	0.70	39	0.36	0.21	0.43	0.59	0.55	0.48	0.30	n.d	n.d	n.d	n.d	n.d	n.d
#1763.27	0.51	0.21	0.11	1.46	0.99	0.40	18	0.36	0.33	0.32	0.15	0.35	0.22	0.48	0.02	0.03	0.01	0.02	0.03	0.00
#1763.55	0.56	0.19	0.09	1.33	0.72	0.34	6	0.48	0.26	0.26	0.36	0.51	0.36	0.16	0.17	0.28	0.13	0.12	0.21	0.00
#1764.10	0.58	0.19	0.12	2.33	1.03	0.53	90	0.21	0.53	0.25	0.03	0.18	0.03	0.22	0.01	0.02	0.00	0.01	0.02	0.00
#1764.65	0.69	0.12	0.06	1.17	0.75	0.35	7	0.43	0.27	0.30	0.49	0.58	0.27	0.03	0.07	0.10	0.06	0.04	0.08	0.00
#1764.90	0.70	0.12	0.06	1.47	1.11	0.40	70	0.25	0.53	0.22	0.03	0.24	0.03	0.16	0.04	0.21	0.03	0.22	0.22	0.01

Table 4 (continued)

Sample ID (m)	Hopanes (µg/g TOC)	Steranes/hopanes	22[S/(S+R)] C$_{31}$ hopanes	Moretane/hopane	Ts/(Ts+Tm)	Gamm./(Gamm.+C$_{30}$ Hop.)	C$_{35}$/C$_{31-35}$ hopanes	Tricyclic terpanes		
								Σ (µg/g TOC)	C$_{19}$/C$_{23}$	C$_{20}$/C$_{23}$
#1756.20	21	0.51	0.59	0.21	0.31	0.05	0.04	4	0.26	0.28
#1756.60	76	0.56	0.59	0.20	0.37	n.d	0.07	16	0.12	0.25
#1757.00	29	0.62	0.60	0.18	0.46	0.06	0.06	6	0.11	0.21
#1757.54	51	0.67	0.60	0.17	0.34	n.d	0.07	13	0.13	0.31
#1757.90	33	0.83	0.60	0.19	0.53	0.07	0.07	10	0.10	0.17
#1758.55	119	0.91	0.61	0.17	0.41	n.d	0.08	32	0.05	0.19
#1759.10	29	0.93	0.61	0.18	0.52	0.12	0.08	11	0.08	0.15
#1759.46	117	0.95	0.60	0.18	0.40	n.d	0.09	33	0.05	0.20
#1759.85	17	1.16	0.61	0.17	0.52	0.10	0.08	6	0.08	0.17
#1760.38	95	0.94	0.60	0.16	0.43	n.d	0.09	24	0.05	0.20
#1760.80	33	0.91	0.59	0.17	0.52	0.09	0.09	10	0.11	0.17
#1761.10	87	1.03	0.60	0.18	0.33	n.d	0.06	25	0.09	0.26
#1761.30	224	0.68	0.61	0.14	0.38	0.02	0.09	48	0.12	0.25
#1761.42	175	0.66	0.60	0.15	0.46	0.02	0.07	44	0.07	0.25
#1761.70	43	0.65	0.60	0.16	0.55	0.08	0.08	12	0.07	0.19
#1761.79	103	0.68	0.60	0.15	0.45	0.02	0.07	31	0.06	0.28
#1761.93	175	0.46	0.61	0.15	0.45	0.02	0.09	38	0.08	0.30
#1762.00	209	0.32	0.60	0.20	0.47	0.02	0.09	40	0.08	0.30
#1762.03	103	0.43	0.60	0.15	0.45	n.d	0.10	21	0.06	0.28
#1762.08	290	0.34	0.59	0.16	0.45	0.02	0.10	52	0.08	0.27
#1762.13	235	0.31	0.60	0.16	0.47	0.02	0.09	41	0.07	0.27
#1762.31	132	0.39	0.60	0.15	0.40	0.02	0.07	41	0.09	0.29
#1762.70	19	0.63	0.59	0.20	0.35	0.07	0.05	5	0.30	0.29
#1762.86	204	0.21	0.59	0.16	0.40	0.07	0.59	25	0.20	0.38
#1763.00	25	0.44	0.58	0.24	0.26	n.d	0.06	8	0.46	0.74
#1763.06	176	0.22	0.60	0.15	0.42	0.02	0.06	30	0.13	0.30
#1763.27	18	1.04	0.54	0.27	0.23	n.d	0.04	6	0.44	0.77
#1763.55	14	0.39	0.60	0.20	0.35	n.d	n.d	6	0.23	0.37
#1764.10	24	3.68	0.54	0.28	0.45	n.d	0.08	9	0.41	1.56
#1764.65	10	0.69	0.60	0.18	0.36	0.06	0.04	9	0.25	0.41
#1764.90	15	4.53	0.51	0.38	0.50	n.d	0.07	8	0.67	1.94

Table 4 (continued)

Sample ID (m)	MP (μg/g TOC)	DMP	MPI-1 (–)	Rc (%)	MDBT (μg/g TOC)	MDR	Rc' (%) Type-I/II	DBT/P	Methylated alkylbenzenes (μg/g TOC)	Aryl-isoprenoids (μg/g TOC)
#1756.20	31	52	0.53	0.72	3	1.63	0.75	0.06	72	7
#1756.60	83	88	0.38	0.63	8	1.54	0.75	0.08	105	26
#1757.00	88	130	0.43	0.66	14	1.29	0.74	0.13	353	49
#1757.54	85	105	0.46	0.68	5	1.56	0.75	0.06	207	50
#1757.90	90	135	0.45	0.67	10	1.49	0.75	0.09	374	65
#1758.55	68	114	0.46	0.67	13	1.44	0.74	0.14	314	84
#1759.10	82	135	0.45	0.67	14	1.48	0.75	0.13	488	83
#1759.46	62	94	0.46	0.68	12	1.47	0.75	0.14	189	52
#1759.85	55	91	0.46	0.68	11	1.34	0.74	0.14	322	53
#1760.38	69	118	0.45	0.67	15	1.30	0.74	0.16	192	53
#1760.80	86	142	0.44	0.66	17	1.45	0.74	0.14	548	92
#1761.10	70	126	0.50	0.70	6	2.06	0.76	0.06	271	61
#1761.30	139	306	0.44	0.66	33	1.17	0.74	0.16	558	121
#1761.42	133	276	0.48	0.69	19	1.51	0.75	0.09	262	63
#1761.70	103	163	0.47	0.68	15	1.57	0.75	0.11	310	60
#1761.79	115	262	0.48	0.69	30	1.30	0.74	0.17	213	53
#1761.93	114	234	0.46	0.68	13	1.75	0.75	0.07	168	41
#1762.00	125	247	0.47	0.68	14	1.67	0.75	0.07	160	40
#1762.03	81	125	0.47	0.68	8	1.69	0.75	0.07	123	32
#1762.08	143	284	0.44	0.66	23	1.46	0.75	0.10	168	43
#1762.13	108	228	0.45	0.67	22	1.33	0.74	0.12	110	28
#1762.31	99	199	0.47	0.68	13	1.54	0.75	0.09	136	0
#1762.70	117	192	0.53	0.72	13	1.89	0.75	0.08	151	16
#1762.86	298	295	0.47	0.68	22	1.79	0.75	0.06	196	28
#1763.00	148	203	0.50	0.70	12	1.74	0.75	0.06	131	16
#1763.06	113	152	0.40	0.64	15	1.30	0.74	0.09	142	25
#1763.27	96	119	0.52	0.71	12	1.72	0.75	0.06	51	7
#1763.55	49	75	0.64	0.78	6	1.69	0.75	0.06	115	10
#1764.10	156	182	0.51	0.71	21	1.96	0.76	0.09	151	26
#1764.65	37	51	0.65	0.79	4	2.19	0.76	0.07	159	15
#1764.90	137	196	0.49	0.70	15	1.71	0.75	0.07	110	15

TOC total organic carbon, *CPI* carbon preference index (Bray and Evans 1961), *Pr* pristine, *Ph* phytane, *dia* methyl diasteranes, *a* C_{27} [diasteranes/sterane], *b* C_{27} [(diasterane/diasterane + sterane)], *MP* Methylphenanthrene, *DMP* dimethylphenanthrene, *MPI-1* Methylphenanthrene Index (Radke et al. 1986), *MDBT* methyldibenzothiophene, *MDR* methyldibenzothiophene ratio (Radke et al. 1986), *Rc* calculated vitrinite reflectance from MDR, *DBT* dibenzothiophene, *Phen* phenanthrene, *AIR* aryl isoprenoid ratio (Schwark and Frimmel 2004)
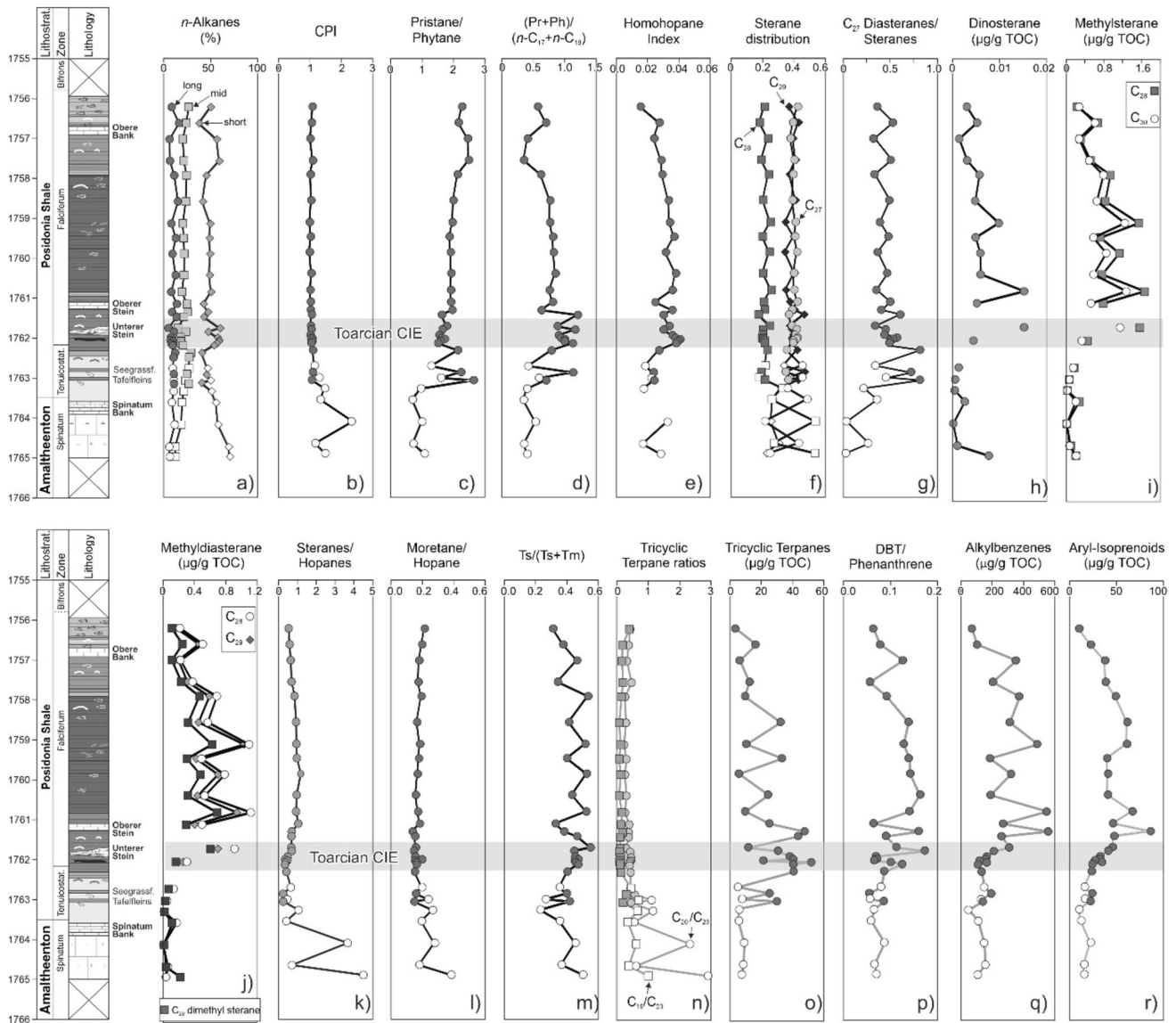
Fig. 9 Concentrations and ratios of selected organic compounds at Salem well showing position of the negative carbon isotope excursion (CIE). Short-chain n-alkanes: n-C_{15-19}/$\sum$ n-alkanes; mid-chain n-alkanes: n-C_{21-25}/$\sum$ n-alkanes; long-chain n-alkanes: n-C_{27-31}/$\sum$ n-alkanes; CPI: carbon preference index (Bray and Evans 1961), sterane distribution: C_{27}/C_{27-29} steranes, C_{28}/C_{27-29} steranes, C_{29}/C_{27-29} steranes; DBT: dibenzothiophene. Low TOC samples below the T-CIE are marked by open symbols

is an additional useful redox parameter, with ratios > 1.75 corresponding to strictly anoxic conditions. On average, Pr/Ph ratios at Salem are slightly higher (1.5–2.6) than at Dormettingen (1.0–2.6), but the (Pr + Ph)/(n-C_{17} + n-C_{18}) ratios are significantly lower (0.3–1.2 versus 0.6–2.5). The low (Pr + Ph)/(n-C_{17} + n-C_{18}) ratios at Salem are clearly a consequence of hydrocarbon generation, which produces much more n-alkanes, than isoprenoids. Moreover, preferential thermal cracking of isoprenoids compared to n-alkanes may also contribute to the decreased values (McNeil and Bement

1996; Zheng et al. 2023). Hydrous pyrolysis experiments showed that thermal stress can also lead to a significant increase in Pr/Ph ratios (Zheng et al. 2023). Therefore, vertical trends of the Pr/Ph and (Pr + Ph)/(n-C_{17} + n-C_{18}) ratios, but not their absolute values, are used for interpretation.
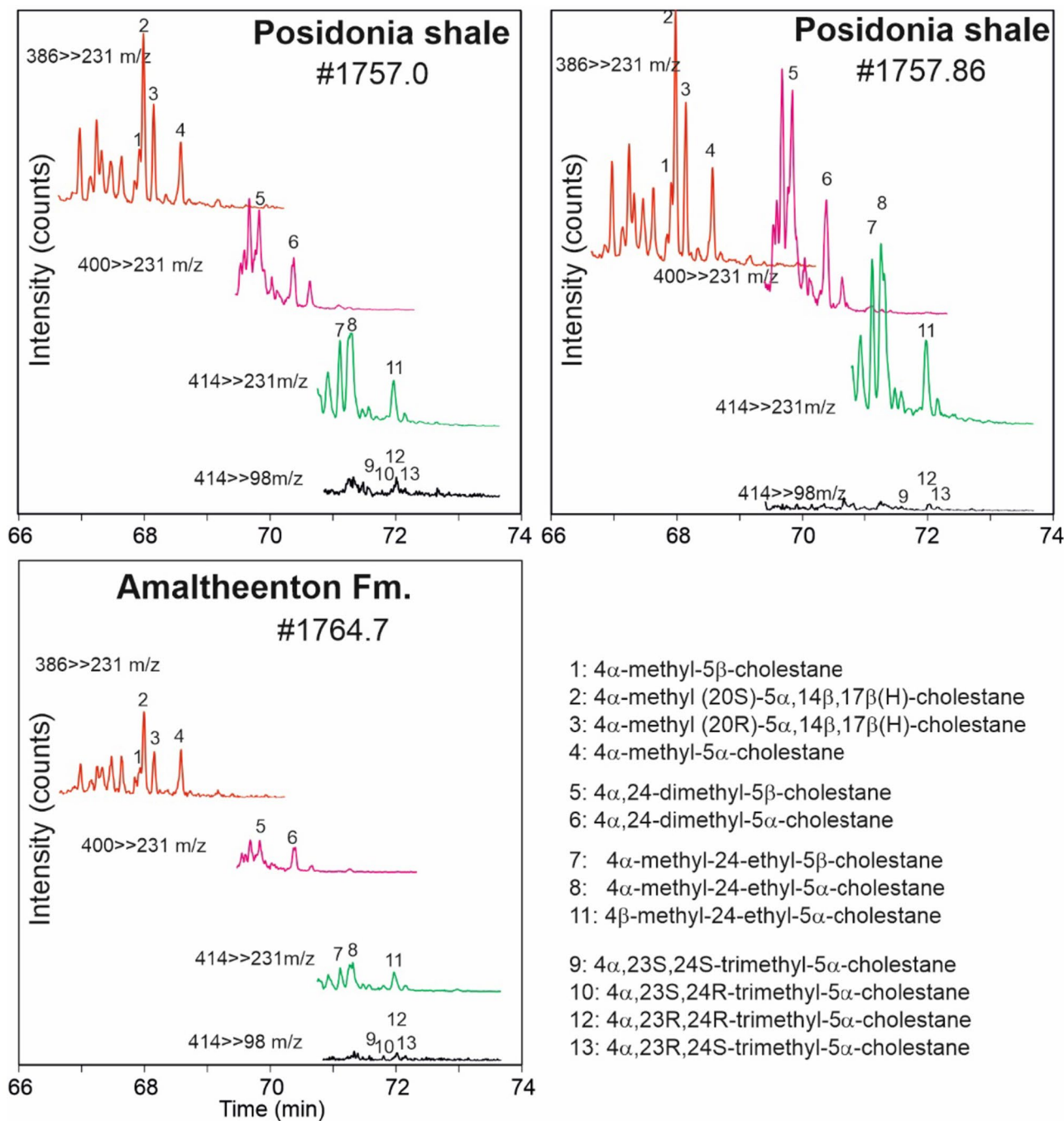
Fig. 10 4-Methylsterane distributions of three samples. Data were acquired by GC–MS/MS. Identification of 4α-methylsteranes, 4β-methylsteranes is based on Goodwin et al. (1988) and Schouten et al. (2000)

Pre-CIE (*spinatum* and *tenuicostatum* zones: 1764.90–1762.31 m)

The lower part of the core (below the T-CIE) is formed predominantly by marly sediments with strong bioturbation indicating oxic conditions (see also Riegraf 1985). Thin limestone layers (Spinatum- or Costatenklalk) and two organic-rich layers (Tafelfleins: 1763.07 m; Seegrasschiefer: 1762.86 m) are intercalated in the background sediments. Organic matter contents are also high in the upper part of this succession (Fleins; 1762.43–1762.31 m), which is considered the basal part of the thick black shale succession.

Table 5 Compound specific carbon isotope ratios (δ^{13}C; ‰) of Upper Pliensbachian and Lower Toarcian sediments from the Salem drill core

| Sample ID [m]	$n\text{-}C_{15}$	$n\text{-}C_{16}$	$n\text{-}C_{17}$	$n\text{-}C_{18}$	$n\text{-}C_{19}$	$n\text{-}C_{20}$	$n\text{-}C_{21}$	$n\text{-}C_{22}$	$n\text{-}C_{23}$	$n\text{-}C_{24}$	$n\text{-}C_{25}$	$n\text{-}C_{26}$	$n\text{-}C_{27}$	$n\text{-}C_{28}$	$n\text{-}C_{29}$	Nor-pristane	Pristane	Phytane
Post-CIE																		
#1756.20	n.d	−30.20	−30.70	−31.40	−31.90	−32.00	−31.80	−31.80	−31.70	−31.90	−31.80	−31.90	−31.70	−31.30	−31.60	n.d	−31.26	−30.25
#1756.60	n.d	−28.39	−31.79	−31.41	−31.83	−32.07	−31.99	−32.21	−32.06	−32.00	−31.75	−31.47	−31.34	−31.86	−32.20	−29.60	−31.33	−29.91
#1757.00	−30.20	−30.30	−31.30	−31.20	−31.30	−31.80	−31.70	−31.90	−31.60	−31.50	−31.90	−32.10	−32.40	−32.30	−32.10	−26.69	−31.82	−30.46
#1757.54	n.d	−31.30	−33.33	−32.85	−33.18	−33.33	−32.94	−33.12	−32.52	−32.61	−32.10	−31.86	−31.46	−32.08	−32.06	−29.35	−31.24	−30.20
#1757.90	−30.40	−30.60	−31.00	−31.70	−31.90	−32.20	−32.10	−32.30	−31.80	−31.40	−31.80	−31.60	−32.00	−31.90	−31.50	−28.36	−31.15	−29.68
#1758.55	−27.85	−30.75	−32.10	−31.73	−32.00	−32.18	−32.07	−32.38	−31.94	−32.08	−31.91	−31.46	−31.72	−31.66	−32.33	−28.71	−30.92	−29.55
#1759.10	−29.70	−30.20	−30.80	−31.10	−31.40	−31.80	−31.80	−31.70	−31.70	−31.50	−31.20	−31.40	−31.70	−32.00	−31.80	−27.26	−30.40	−29.01
#1759.46	n.d	−29.31	−31.40	−31.42	−31.80	−32.11	−31.79	−32.04	−31.57	−31.63	−31.67	−31.16	−31.16	−31.70	−32.23	−28.42	−30.63	−29.41
#1759.85	−30.50	−30.90	−31.30	−31.40	−31.50	−32.10	−31.70	−32.10	−31.80	−32.10	−31.60	−32.00	−32.00	−32.30	−31.90	−27.11	−30.02	−28.89
#1760.38	−25.14	−30.09	−31.88	−31.62	−31.84	−32.30	−31.92	−32.12	−31.97	−31.83	−31.50	−31.36	−31.31	−31.28	−32.29	−27.36	−30.27	−29.35
#1760.80	−29.90	−30.40	−30.90	−31.50	−31.90	−31.60	−31.40	−31.70	−31.80	−31.70	−32.00	−31.70	−32.20	−31.70	−31.50	−28.82	−30.81	−30.09
#1761.10	−27.39	−30.06	−31.69	−31.29	−31.59	−31.84	−31.50	−31.79	−31.49	−31.67	−31.13	−31.08	−31.04	−31.35	−32.05	−27.53	−30.17	−28.86
#1761.30	−30.22	−31.70	−32.26	−31.90	−32.08	−32.31	−32.20	−32.37	−31.80	−31.84	−31.43	−31.42	−31.29	−31.22	−31.72	−28.74	−29.90	−29.52
#1761.42	−28.60	−30.64	−32.13	−32.07	−31.94	−32.50	−32.20	−32.36	−32.08	−32.28	−31.69	−31.76	−31.33	−31.34	−31.62	−29.37	−32.16	−31.08
T-CIE																		
#1761.70	−30.10	−30.80	−31.10	−31.60	−31.70	−31.70	−31.50	−31.10	−31.40	−31.60	−31.70	−32.20	−32.10	−32.30	−31.60	−29.86	−32.11	−30.92
#1761.79	−29.38	−31.39	−32.50	−31.64	−32.27	−32.88	−32.64	−32.60	−32.23	−32.31	−31.77	−32.08	−32.00	−31.96	−32.13	−29.72	−32.20	−31.07
#1761.93	−30.66	−31.67	−32.55	−32.55	−33.22	−33.79	−34.83	−35.23	−35.01	−35.00	−34.27	−33.94	−34.73	−34.92	−34.19	−29.29	−31.82	−30.70
#1762.00	−30.85	−32.04	−32.67	−32.17	−32.29	−33.02	−35.09	−34.08	−34.47	−35.10	−34.01	−34.55	−34.92	−34.84	−34.23	−29.04	−31.97	−31.04
#1762.03	n.d	−32.78	−32.97	−32.62	−33.10	−33.30	−33.38	−33.40	−33.14	−33.26	−33.06	−34.16	−32.77	−32.10	−34.04	n.d	−30.69	−30.73
#1762.08	−30.03	−31.87	−32.37	−32.47	−33.60	−34.42	−34.19	−34.92	−34.97	−34.73	−34.00	−34.36	−34.62	−35.17	−33.98	−28.79	−31.92	−30.68
#1762.13	−32.50	−32.43	−32.52	−33.90	−34.94	−34.54	−34.75	−34.55	−35.93	−34.28	−34.34	−34.20	−34.12	−35.32	−33.82	−29.22	−32.32	−31.47
Pre-CIE																		
#1762.31	−30.87	−32.52	−33.27	−34.14	−34.30	−34.72	−34.78	−34.15	−33.48	−33.35	−32.82	−32.06	−31.86	−31.88	−32.31	−28.12	−31.62	−30.46
#1762.70	n.d	−31.20	−31.50	−31.90	−32.10	−32.30	−32.10	−31.80	−31.40	−31.40	−31.60	−31.40	−31.00	−31.10	−31.50	n.d	−29.82	−29.50
#1762.86	−27.41	−30.91	−31.57	−31.33	−31.43	−31.76	−31.61	−31.66	−31.53	−31.78	−31.41	−31.73	−31.29	−31.01	−31.03	−28.96	−31.35	−30.19
#1763.06	−29.70	−31.46	−32.34	−32.00	−31.87	−32.26	−32.13	−32.43	−32.24	−32.67	−32.15	−32.59	−31.82	−31.59	−31.89	−30.23	−32.57	−31.14
#1763.27	n.d	n.d	n.d	n.d	−30.84	−31.22	−31.81	−31.70	−31.54	−31.55	−31.46	−30.92	−30.60	−29.81	−29.09	n.d	n.d	n.d
#1763.55	n.d	n.d	−30.50	−31.00	−31.30	−31.00	−30.30	−29.50	−29.30	−29.30	−28.80	−28.90	−29.20	−29.00	−29.20	−26.52	−31.43	−30.22
#1764.65	n.d	n.d	−29.70	−30.40	−30.60	−30.40	−29.80	−29.50	−28.50	−28.20	−28.20	−28.70	−28.50	−28.30	−28.80	−25.90	−30.21	−29.38
#1764.90	n.d	n.d	−27.36	−30.34	−30.72	−30.59	−30.02	−29.98	−28.92	−29.26	−28.15	−28.30	−27.92	−27.45	−27.02	−28.04	−29.93	−30.05
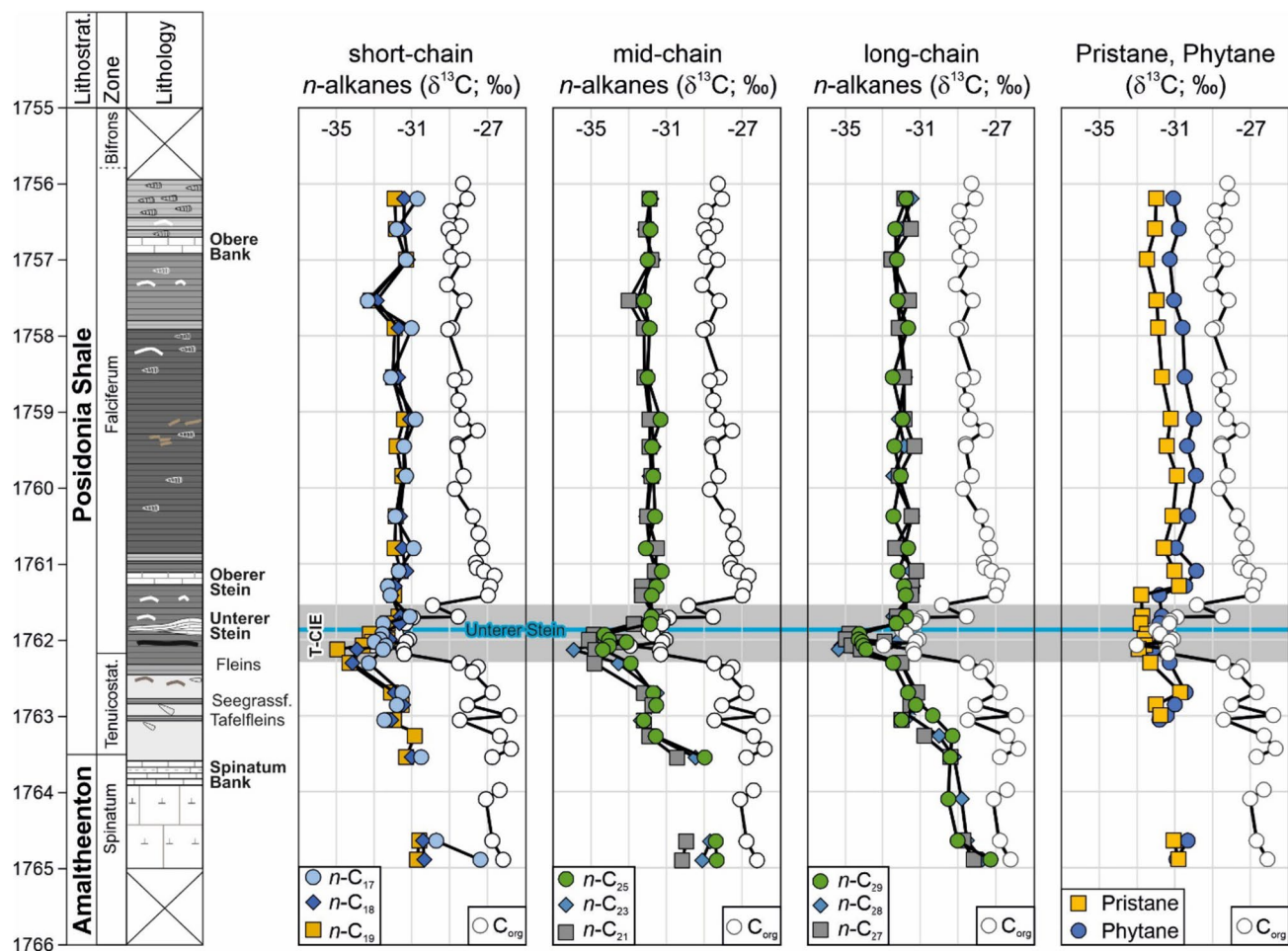
Fig. 11 Depth plot representation of variation in $\delta^{13}C$ of *n*-alkanes, pristane, and phytane. Vertical variation of bulk carbon isotope values ($\delta^{13}C_{org}$) is shown for comparison. The position of the "Unterer Stein" marker bed (blue line) and the T-CIE (grey rectangle) are highlighted

The prevailing oxic conditions resulted in low TOC contents in the background marls.

The HI of low-TOC sediments (<0.6 wt%) ranges from 33 to 173 mgHC/gTOC suggesting the presence of terrigenous or strongly degraded marine organic matter. Relatively high contributions of land plants are also indicated by the lowermost two palynofacies samples (#1763.00; #1762.70), macerals data, and geochemical parameters [elevated CPI; Bray and Evans 1961 (Fig. 9b); high C_{20}/C_{23} and C_{19}/C_{23} tricyclic terpane ratios, Noble et al. 1986; Peters et al. 2005; French et al. 2014 (Fig. 9n)]. Low (Pr + Ph)/(n-C_{17} + n-C_{18}) ratios of the bioturbated sediments agree with an oxygenated environment (e.g., Frimmel et al. 2004). In contrast, low Pr/Ph ratios (<0.6) pretending strictly anoxic conditions clearly must not be considered for interpretation. A change in compound specific isotope (CSI) patterns (Fig. 11) between Pliensbachian (1764.90–1763.55 m) and Toarcian pre-CIE samples (1763.55–1762.31 m) may be related to a change in organic matter input.

Both, the organic matter-rich Tafelfleins and the Seegrassschiefer are bioturbated. Nevertheless, TOC contents (2.68 and 1.84 wt%, respectively) and HI values (423 and 358 mgHC/gTOC) are high. This suggests a high amount of aquatic organic matter and relatively good organic matter preservation despite bioturbation. The higher HI values, as well as CPI values and C_{20}/C_{23} and C_{19}/C_{23} tricyclic terpane ratios, which are lower than those in the adjacent organic-poor sediments indicate the higher amount of aquatic organic matter. Similar to the low-TOC samples, the redox parameters yield contradicting results. However, it is obvious that oxygen-depleted conditions occurred during deposition. The prevailing trace fossil is *Chondrites* (Riegraf 1985; Röhl and Schmid-Röhl 2005), which is well known from anaerobic and dysaerobic deposits (Bromley and Ekdale 1984). Seilacher (1990) and Fu (1991) suggested that the trace maker of *Chondrites* is a chemosymbiotic bivalve living at the aerobic/anaerobic interface, which pumps methane and hydrogen sulphide from the sediments (see also Uchman and Wetzel 1999; Izumi 2012; Baucon
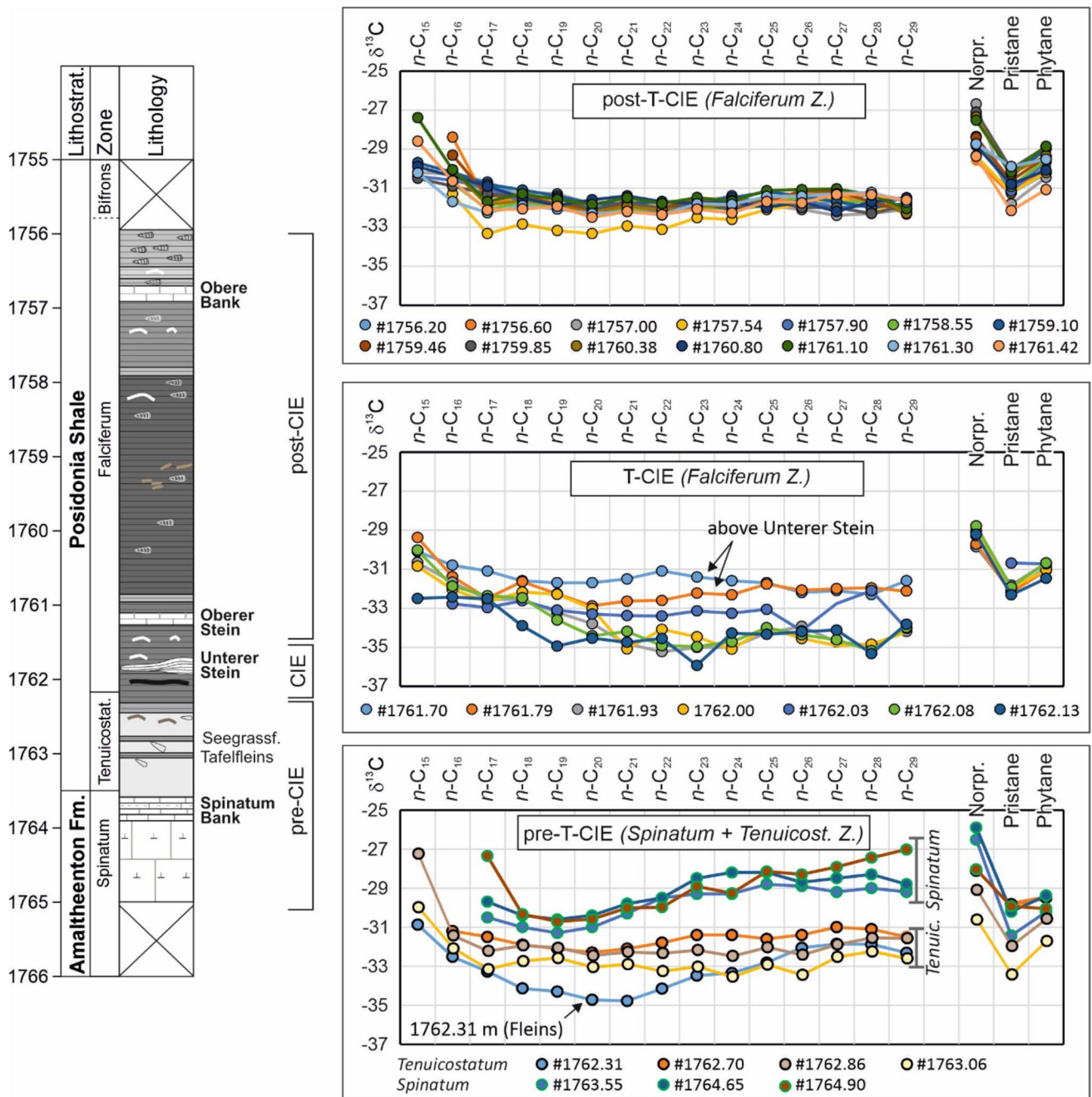
Fig. 12 Carbon isotope composition of individual *n*-alkanes and isoprenoids for samples from different stratigraphic intervals in the Salem section

et al. 2020). In any case, bioturbation did not result in significant organic matter degradation. In the upper part of the *tenuicostatum* Zone (*semicelatum* Subzone), TOC contents increase gradually and reach 3.68 wt% at 1762.31 m (Fleins). Pr/Ph and (Pr + Ph)/(n-C_{17} + n-C_{18}) ratios as well as the homohopane index (HHI; Peters and Moldowan 2001) suggest oxygen-depleted, but not yet strictly anoxic conditions, which were established only during the T-CIE. Sample

S08 (1762.43 m) from this interval records a drastic reduction in dinoflagellate diversity. The occurrence of *Mendicodinium* sp. at 1762.43 m depth (sample S08; inteval A), before the complete dinoflagellate cysts demise, is striking. In the Posidonia Shale (SW Germany), before the inception of the fully anoxic conditions, *Mendicodinium spinosum perforatum* was recorded in the lowermost *falciferum* Zone, which was described as the last taxon able to survive the initial,
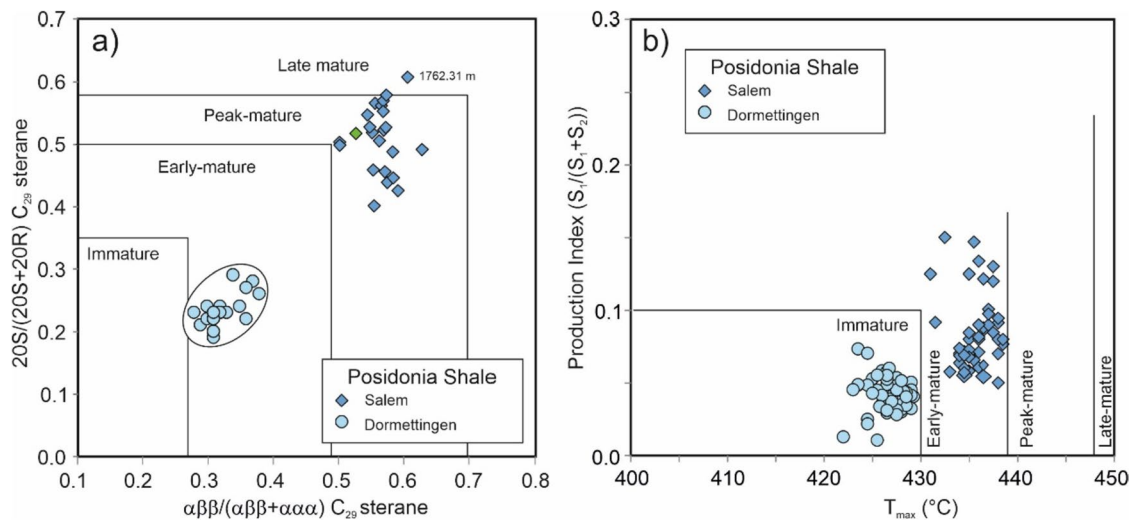
Fig. 13 Cross plots of **a** 20S/(20S + 20R) isomer ratios of $\alpha\alpha\alpha$ C$_{29}$ steranes versus $\alpha\beta\beta$/($\alpha\beta\beta$ + $\alpha\alpha\alpha$) C$_{29}$ steranes (boundaries between maturity fields after Peters et al. 2005) and **b** production Index versus T_{max} for Posidonia Shale at Salem and Dormettingen (boundaries between T_{max}-based maturity fields for Posidonia Shale according to Song et al. 2015)

Table 6 Thickness, genetic potential (S$_1$ + S$_2$), and Source Potential Index (SPI) of different stratigraphic units at Salem and Dormettingen

	Net thickness (m)	Average S$_1$ + S$_2$ (mgHC/g rock)	SPI (tHC/m^2)	References
Southwest German Basin				
Salem				This study
Bifrons Z	3.0	Interval not cored	0.30 (estimated)	
Falciferum Z	6.43	28.94	0.49	
			Total: ~0.8	
Dormettingen				Ajuaba et al. (2022)
Bifrons Z	4.0	50.21	0.53	
Falciferum Z	4.2	52.10	0.58	
			Total: 1.11	
1026	11.7	32.7	0.98	Littke et al. (1991b)
1022	11.6	32.2	0.95	Littke et al. (1991b)
1003	12.1	27.9	0.86	Littke et al. (1991b)
1005	8.6	25.4	0.56	Littke et al. (1991b)
Northwest German Basin				
Wickensen	30.6	72.09	5.83	Burnaz et al. (2024)

Data for additional wells in the Southwest and Northwest German Basin are given for comparison

severe environmental conditions as a consequence of the T-OAE (Galasso et al. 2022).

T-CIE (uppermost *tenuicostatum* and lower *falciferum* zones: 1762.25–1761.50 m)

The T-CIE interval in the Salem is very thin (~0.75 m). Strongly oxygen-depleted conditions during the T-CIE are evidenced by the presence of laminated black shales and the absence of benthic faunas (Röhl and Schmid-Röhl 2005). Anoxic conditions are also shown by relatively low

Pr/Ph ratios (1.54–1.82; Fig. 9c), relatively high (Pr + Ph)/(n-C$_{17}$ + n-C$_{18}$) (0.88–1.17; Fig. 9d) and high C$_{35}$ HHI (0.03–0.04; Fig. 9c). The presence of aryl-isoprenoids, which have been used as proxies for photosynthetic sulphide-oxidising bacteria (Summons and Powell 1987), indicates photic zone anoxia (Schouten et al. 2000; Frimmel et al. 2004; Schwark and Frimmel 2004). At Salem, the concentration of aryl-isoprenoids increases upwards within the T-CIE (Fig. 9r). The concentrations of methyl-alkylbenzenes and aryl-isoprenoids show a positive correlation (r^2 = 0.81) and show similar depth trends within the T-CIE (Fig. 9q).

Probably, both compound groups formed by the degradation of carotenoids (e.g., isorenieratene). Alternative formation mechanisms include direct cyclisation and aromatisation of straight chain fatty acids (Derenne et al. 1990; Chairi et al. 2010). The maximum methyl-alkylbenzenes concentration in Salem (548 μg/g TOC; 1760.80 m) is ten times higher than for Dormettingen (51 μg/g TOC; Ajuaba et al. 2022). This suggests a maturity effect on the degradation of aromatic carotenoids or the cyclization and aromatization. As elevated amounts of alkylbenzenes have been recorded in sediments deposited during periods of enhanced salinity (Sinninghe-Damsté et al. 1993; Chairi et al. 2010), it is possible that their elevated amounts within (and above) the T-CIE in the Salem section were triggered by salinity stratification and water column anoxia. However, the gammacerane index is typically low (Table 4) suggesting only weak salinity stratification. In contrast, the DBT/P ratio, a proxy for free H_2S in the water column or the pore water (Hughes et al. 1995), varies strongly in the T-CIE, but is generally high (Fig. 9p).

Strictly anoxic conditions resulted in high TOC contents (4.78–7.44%), which are below 2 wt% only in the "Unterer Stein" marker bed (1.62 wt%; 1761.83 m). High HI values (538–634 mgHC/gTOC; Fig. 3g) reflect the dominance of aquatic organic matter and the excellent preservation conditions. The observed upward increase in the concentration of aryl-isoprenoids (and methyl-alkylbenzenes) together with slightly lower HHI values may indicate oxygen-depletion above the "Unterer Stein". Increased oxygen-depletion probably caused slightly higher HI values above the "Unterer Stein" (average 618 mgHC/gTOC) compared to the interval below this marker (574 mgHC/gTOC). Alternatively, the slightly lower HI below the "Unterer Stein" may indicate greater terrigenous organic matter input during the early T-CIE, as indicated macroscopically by a thin coaly layer and microscopically by relatively high amounts of translucent phytoclasts in the sample at 1762.03 m depth (Table 2) and vitrinite in the sample at 1761.93 m depth (Table 3). In contrast, terrigenous phytoclasts or macerals are very rare in samples above the "Unterer Stein". Similar to Dormettingen (Galasso et al. 2021), dinoflagellate cysts were not recorded in the T-CIE (lower part of palynofacies B; Figs. 4, 5).

TOC contents in the T-CIE at Salem reach 7.44%. This value is high, but lower than in the same interval at Dormettingen (~ 10 wt%; Fig. 1c) and in post-CIE sediments in the Salem core (max. 8.95 wt%; see below). As the low thickness of the T-CIE contradicts a dilution of organic matter by high clastic input, and the similar high HI values in the T-CIE and post-CIE sediments contradict variations in organic matter preservation, it is likely that the relatively low TOC content in the T-CIE is due to limited organic productivity (see also Littke et al. 1991b). Sterane/hopane ratios have been used to estimate paleo-productivity of phytoplankton (Schulz et al. 2002). Thus, the observed low ratios in the T-CIE interval

(Fig. 9k) support this interpretation. In this connection, it should be noted that only stratigraphic trends of the sterane/hopane ratio, but not absolute values are considered, because the sterane/hopane ratio decreases significantly with maturity (Zheng et al. 2023). Thus, it is not surprising that the sterane/hopane ratio is significantly lower in Salem (0.21–1.16) than in Dormettingen (1.01–6.32; Ajuaba et al. 2022).

The concentrations of 4-methylsteranes including dinosteranes and 4-methyl-diasteranes have been determined only for a limited sample set. These compounds are generally ascribed to dinoflagellates (Withers 1987; Moldowan and Talyzina 1998; Volkman et al. 1990) and show similar depth trends (Fig. 9h–j) with maxima in the upper part of the T-CIE. Consequently, despite the generally low phytoplankton productivity, it is likely that the productivity of non-cyst-forming dinoflagellates was relatively high in the upper part of the T-CIE.

Post-CIE (upper *falciferum* Zone: 1761.50–1756.00 m)

Based on TOC trends, the post-CIE sediments are subdivided into four units. Environmental proxies are discussed separately for each of them starting with the lower unit I.

Unit I (1761.5–1761.0 m) includes the "Oberer Stein" marker and is slightly bioturbated in its upper part. An increase in oxygen availability at 1761.30–1761.10 m is also indicated by Pr/Ph ratios, the HHI and the concentration of aryl-isoprenoids. HI values in unit I vary considerably (455–630 mgHC/gTOC). The sample with the minimum HI (#1761.10) contains a very low amount of terrigenous organic matter (Fig. 4). This shows that varying HI values reflect varying oxygen availability rather than changes in organic matter input. Similar to the sediments deposited during the T-CIE, dinoflagellate cysts are missing (palynofacies interval B sensu Galasso et al. 2021).

Unit II (1761.0–1757.9 m) is an approximately 3-m thick interval that includes the highest TOC contents (4.71–8.95%) in the studied profile (Fig. 3d). Overall, there is a slight upward decrease in TOC (from ~ 9 to ~ 6%). Sterane/hopane ratios reach a maximum at 1759.85 m depth and decrease upwards (Fig. 9k). This suggests that high TOC contents are due to enhanced phytoplankton productivity. The highest amount of marine POM is recorded at 1760.80 m depth. Beyond this point, the input of terrigenous POM experiences only a minor increase (Fig. 4), but the marine/terrestrial ratio remains high. This is also reflected by uniformly high HI values (557–660 mgHC/gTOC). Tasmanaceae algae are present in both POM and maceral assemblages, while dinoflagellate cysts are absent. Belemnite remains, which are absent in the T-CIE and in unit I, reappear in small number in unit II.

The redox parameters (Pr/Ph; (Pr + Ph)/(n-C_{17} + n-C_{18}); HHI) suggest strongly reduced oxygen availability, with a subtle trend towards less strictly anoxic conditions in the upper part of the succession. This agrees with the observed increase in belemnite remains and the presence of some shell layers. Concentrations of aryl-isoprenoids are generally high and even more so in the upper part of Unit II. Overall, redox parameters and high TOC contents suggest that the degree of oxygen-depletion during deposition of unit II was in a similar range compared to the T-CIE. This differs from the condition observed in the Dotternhausen (Schwark and Frimmel 2004) and Dormettingen (Ajuaba et al. 2022) sections, where the maximum oxygen depletion occurred during the T-CIE just above the "Unterer Stein". The availability of free H_2S is evidenced by high DBT/Phen ratios. The high sulphur contents (max. 4.31% at 1760.38 m) agree with this interpretation. Despite of anoxic marine conditions, TOC/S ratios are high in the upper 1.2 m of unit II (3.8–5.1). This may indicate an increase in freshwater runoff.

Unit III (1757.9–1757.0 m) starts with a bioturbated layer and includes some shells. TOC contents (2.92–4.04%) and HI values (462–523 mgHC/gTOC) are relatively low. Bioturbation and the stratigraphic trends of biomarker proxies (Fig. 9c, d, e, r) show that this reflects an increase in oxygen availability. *Unit IV* (1757.0–1755.0 m) follows above the "Obere Bank" limestone marker. The presence of several bioturbated horizons and the high number of belemnites show a well oxygenated environment. Consequently, TOC (1.68–3.16 wt%) and HI (296–464 mgHC/gTOC) are even lower than in unit III. The organic matter input during deposition of units III and IV is characterised by an increasing fraction of terrigenous organic material (Figs. 4, 9n). Sterane/hopane ratios (Fig. 9k) are also decreased in units III and IV suggesting reduced phytoplankton productivity. *Sphaeropollenites* sp. and prasinophytes are common (palynofacies C sensu Galasso et al. 2021; Fig. 4), but dinoflagellate cysts are still absent.

Comparison with other Toarcian sections in the SWGB

The position of marker beds and the T-CIE in the Salem core enable detailed correlation with other Toarcian sections in the SWGB. In addition to examining variations in lateral thickness, this section delves into an investigation of both similarities and differences among depositional environments.

It is noticeable that the lower part of the Posidonia Shale at Salem is very thin. For example, the sediment succession between the top of the Spinatum Bank and the "Oberer Stein" is only 2.4 m thick. In contrast, this same interval in the Dotternhausen/Dormettingen area, located about 65 km NW of Salem, is more than twice as thick (~5.5 m;

Fig. 14). The transition of the Amaltheenton Formation to the Posidonia Shale is gradual and there is no sign of an erosional unconformity at the base of the Posidonia Shale, as recently described by Arp et al. (2021) in the Franconian Alb (Ludwigskanal section; Fig. 1a). The only stratigraphic layer, which is absent in the lower Posidonia Shale at Salem is the "Steinplatte" near the top of the T-CIE (e.g. Ajuaba et al. 2022; Fig. 1c). The latter marker bed, however, is not as continuous as the "Oberer Stein" and is absent, for example, in the German-Swiss border area (e.g., Aselfingen; Riegraf 1985; Fernandez et al. 2021) and east of Reutlingen (Stuttgart; Riegraf 1985). Moreover, each stratigraphic unit (including the T-CIE) is thinner at Salem compared to Dormettingen (Fig. 14). Thus, the thinness of the lower part of the Posidonia Shale is clearly not due to non-deposition or erosion of specific layers. Thickness variations were also observed by Riegraf (1985), who interpreted these as consequences of deposition in paleo-basins and paleo-swells. Based on this interpretation, it is evident that the Salem section was likely deposited within an early Toarcian paleo-swell, and a potential connection to the Vindelician High is plausible.

While the thickness of the Lower Posidonia Shale at Salem is less than elsewhere, the thickness of the middle part of the Posidonia Shale (i.e., interval between "Oberer Stein" and "Obere Bank"; ~4.2 m) is thicker than in the Dotternhausen/Dormettingen area (~1.5 m; Fig. 14). In the latter area the "Inoceramen Bank", marking the *falciferum/bifrons* boundary occurs roughly 60 cm above the "Obere Bank". In the Salem core, this marker is absent, but probably lies just above the core interval. Thus, the total thickness of the *falciferum* Zone probably slightly exceeds 5 m. This exceeds the thickness observed in most sections in the SWGB and indicates increased subsidence during deposition of the upper part of the *falciferum* Zone (units II-IV of the post-CIE sediments).

The *bifrons* Zone in the Salem borehole is about 3 m thick, but was not cored. This is less than the thickness measured at Dormettingen, where it spans about 4.4 m (Galasso et al. 2021, 2022). However, it is important to note that, the thickness of the *bifrons* Zone in the SWGB varies considerably due to late Toarcian erosion. In some areas, such as the northeast Swabian Alb (locations like Gingen/Fils and Göppingen; Fig. 1b), this erosion has led to the complete removal of the entire *bifrons* Zone and has even cut down to the "Oberer Stein" horizon (within the *elegans* Subzone; e.g. Riegraf 1985). Since the *bifrons* Zone and the boundary with the overlying upper Toarcian sediments were not cored in the Salem borehole, it is impossible to determine whether the upper part of the Posidonia Shale was affected by erosion in this specific location.

The changes in depositional environment are largely synchronous in the Salem and in the Dormettingen/

Dotternhausen areas, which is also reflected by similar TOC trends (Fig. 14). In both areas, a peak in oxygen depletion is observed during the T-CIE shortly after deposition of the "Unterer Stein". However, at Salem, following a short period with deposition of bioturbated sediments, anoxia continued during the early *falciferum* Subzone (unit II of the post-CIE sediments) and caused TOC contents, which are even higher than in the T-CIE. In addition, the dinoflagellate cyst blackout (Prauss and Riegel 1989, 1996; Prauss et al. 1991), which is restricted to upper *exaratum* and lower *elegans* subzones at Dormettingen (Galasso et al. 2022; Fig. 1c), continued in the *falciferum* Subzone at Salem. Similarly, Prauss et al. (1991) noted that the entire bituminous facies within the *falciferum* and *bifrons* zones in borehole Bisingen/Zimmern #1002, situated approximately 20 km northeast of Dormettingen (Fig. 1b), showed virtually no presence of dinocysts. The extended absence of dinoflagellate at Salem may be a result of continuing anoxia during the *falciferum* Subzone or its proximal setting resulting in increased turbidity and low salinity.

Bulk and compound-specific carbon isotope data

Bulk organic carbon isotope ratios

Bulk organic carbon isotope ratios ($\delta^{13}C_{org}$) in the Salem section (− 25.7 to − 33.1‰) are similar to those at Dormettingen (Fig. 14). The lowermost part of the black shale interval (1762.43–1762.31 m) shows $\delta^{13}C_{org}$ values (− 27.49 to − 28.49‰) similar to those of the underlying Tafelfleins and the Seegrasschiefer (− 28.06 to − 28.48‰). The largest drop in $\delta^{13}C_{org}$ occurs between 1762.31 (Fleins) and 1762.19 m (− 31.39‰). A depth of ~ 1762.25 m, therefore, has been accepted as the base of the T-CIE, while the top of the T-CIE is at ~ 1761.50 m. Although the T-CIE at Salem is much thinner (0.75 m) than at Dormettingen (~ 2.8 m), its amplitude falls within a similar range (5–6‰). A similar strong negative CIE has been determined in the Cleveland Basin (5–7‰), while the CIE is smaller in the Paris (3.7‰), Iberian (~ 3‰) and Sichuan basins (~ 4‰) (see Ajuaba et al. 2022 and references therein). A very strong negative CIE has also been recorded for well Schandelah in the Northwest German Basin (~ 7‰; van de Schootbrugge et al. 2019), where the T-CIE is also remarkably thin (1.4 m).

Stable carbon isotope ratios of *n*-alkanes

As expected, $\delta^{13}C$ ratios of *n*-alkanes also show a shift in the T-CIE, but the negative shift (3–4‰) is lower compared to that observed for $\delta^{13}C_{org}$. Moreover, there are some interesting differences between trends of $\delta^{13}C_{org}$ and $\delta^{13}C$ of different *n*-alkanes.

As stated above, the base of the T-CIE is located above the Fleins (1762.31 m) based on $\delta^{13}C_{org}$. This interpretation is also valid for long-chain *n*-alkanes (Fig. 11). However, it appears that the CIE begins slightly earlier (during deposition of the Fleins) for short-chain *n*-alkanes (up to *n*-$C_{21/22}$) (Figs. 11, 12). While long-chain *n*-alkanes may be derived from landplants, short-chain n-alkanes are typically derived from algae and other aquatic organisms (Eglinton and Hamilton 1967). Hence, this result suggests that isotopically light CO_2 was first recorded in the aquatic environment.

The $\delta^{13}C$ values of *n*-alkanes in the upper part of the T-CIE (above the "Unterer Stein"; #1761.79, #1761.70) are significantly less negative than those in the lower part (below the "Unterer Stein"; #1762.13 to #1761.93) and similar to post-CIE background values (Figs. 11, 12). Similar to Dormettingen, redox-sensitive parameters suggest a higher degree of oxygen-depletion above the "Unterer Stein". This supports the temporal decoupling of the maximum isotope excursion and the strongest basin restriction as postulated based on isotope ratios of pristane and phytane in the Dormettingen section (Ajuaba et al. 2022; Fig. 1c).

No systematic variation between $\delta^{13}C$ ratios of *n*-alkanes in the mature Salem core and the immature Dormettingen section can be observed. For example, $\delta^{13}C$ ratios of *n*-alkanes from the *teniucostatum* Zone are slightly more negative than those at Dormettingen, while those from the falciferum Zone (including the T-CIE) are slightly less negative. This suggests that maturity has a no significant effect on $\delta^{13}C_{alkanes}$ (see also Pedentchouk and Turich 2017).

Stable carbon isotope ratios of pristane and phytane

At Dormettingen, the amplitude of the CIE of pristane and phytane is about 4.5‰ and $\delta^{13}C_{isoprenoid}$ values increase continuously upwards within the T-CIE. A similar trend was expected for Salem, but the amplitude of the CIE is only 2‰ and no clear depth trend is observable (Fig. 11). Indeed, the most negative $\delta^{13}C_{pristane}$ value is recorded for the Tafelfleins (1763.06 m) in the pre-CIE interval and not for the T-CIE.

No correlation between $\delta^{13}C$ of isoprenoids and *n*-alkanes could be established. This might indicate that pristane and phytane are not derived from the phytol side chain of chlorophyll of aquatic or terrestrial plants. Frimmel et al. (2004) suggested that the surprisingly high Pr/Ph ratios in Posidonia Shale may be due to secondary input of pristane from tocopherol or chromanes. However, as tocopherol- and chromane-derived pristane has the same $\delta^{13}C$ as the phytol side chain (Hughes et al. 1995; Grice et al. 1998; Peters et al. 2005; Zhang et al. 2012), it is expected to have a minor influence on isotope data. This is also supported by the excellent correlation exists between $\delta^{13}C_{pristane}$ and $\delta^{13}C_{phytane}$ at Dormettingen (Ajuaba et al. 2022) and Salem. It should be added that an effect of hydrocarbon migration on $\delta^{13}C$ of
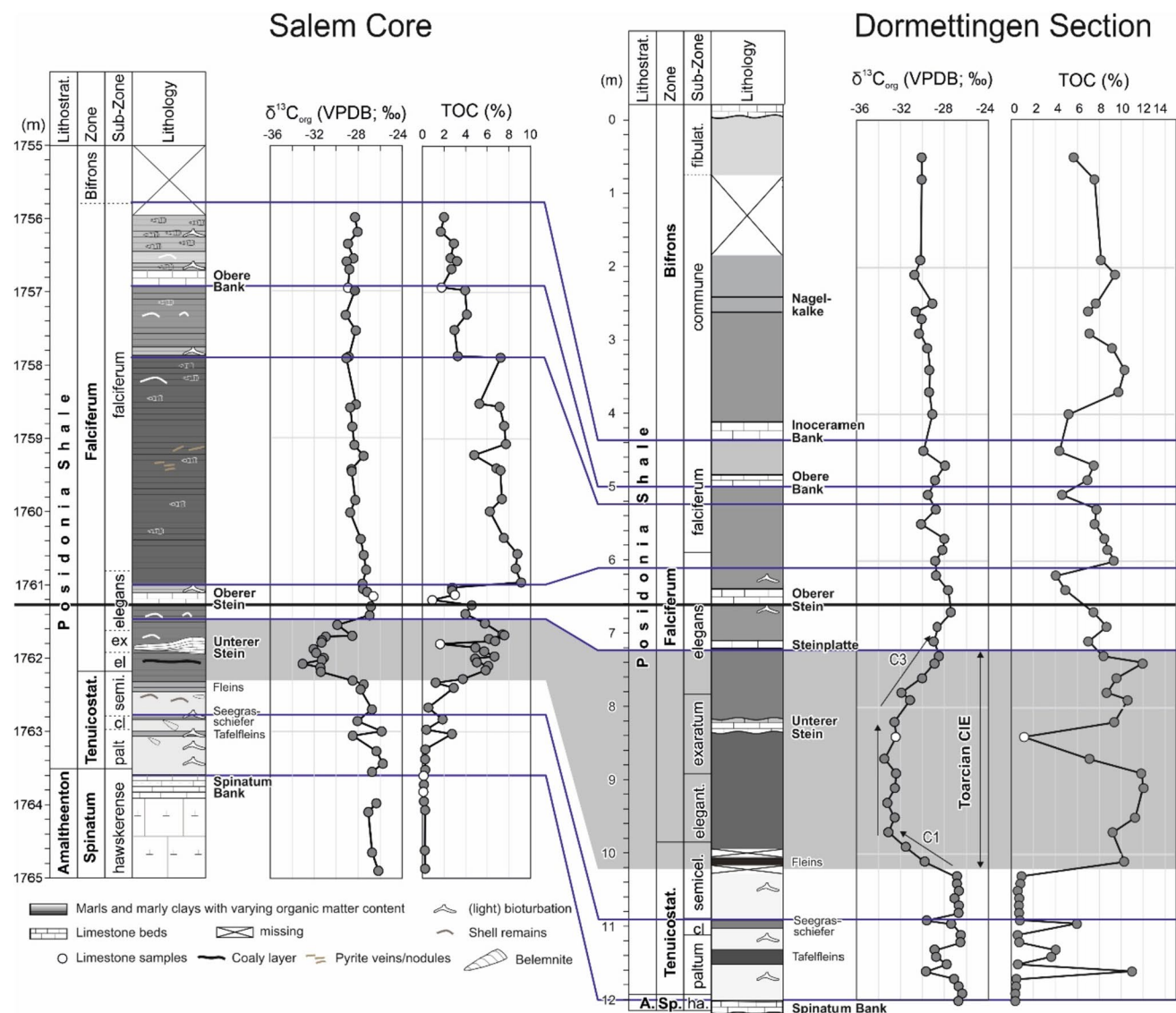
Fig. 14 Correlation of the Salem drill core with the Dormettingen section. Datum is the base of the "Oberer Stein" marker bed. Note the lower thickness of the lower part of the Posidonia Shale and the higher thickness of the upper part (*falciferum* Subzone) in the Salem core. Data from the Dormettingen section are from Galasso et al. (2021) and Ajuaba et al. (2022)

pristane and phytane can be excluded, as isoprenoids are less mobile than *n*-alkanes (e.g., Leythaeuser et al. 1982; Zhang et al. 2023; Zheng et al. 2023). Hence, additional investigations are necessary to determine the factors controlling δ^{13}C values of pristane and phytane at Salem.

Conclusion

A total of 62 core samples were collected from the Salem borehole in southwestern Germany to assess the depositional environment and petroleum potential of the lower Toarcian Posidonia Shale beneath the North Alpine Foreland Basin.

The most important results of the comprehensive geochemical and petrographic investigation are summarized below.

The Salem core spans the *tenuicostatum* and *falciferum* ammonite zones of the Posidonia Shale and the uppermost 1.5 m of the underlying Pliensbachian Amaltheenton Formation. The upper part of the Posidonia Shale (*bifrons* Zone), which is about 3 m thick was not cored.

Compared to the Dormettingen section, located about 65 km NW of Salem, the thickness of the lower part of the Posidonia Shale (*tenuicostatum* Zone to *elegans* Subzone of the *falciferum* Zone) is sigificantly thinner, while the thickness of the *falciferum* Subzone is greater. This suggests sigificant changes in basin geometry at the *elegans/falciferum* boundary.

As observed in many Toarcian sections, the strongest oxygen depletion occurred during deposition of the upper part of the T-CIE (above "Unterer Stein"). However, strong anoxia also occurred during deposition of the post-CIE sediments. This together with higher productivity resulted in peak TOC values in the uppermost *elegans* and lower *falciferum* subzones. The dinoflagellate cyst blackout lasted throughout the entire *falciferum* Zone, likely as another consequence of significant oxygen-depletion.

The T-CIE interval at Salem is very thin (0.75 m), but the amplitude of the CIE ($\delta^{13}C_{Corg}$) is similar to other section in the SWGB (~ 5 to 6‰). The T-CIE is less pronounced for *n*-alkanes (3–4 ‰).

Similar to Dormettingen, an obvious time shift exists between the isotopic minimum ($\delta^{13}C_{alkanes}$) and peak anoxic conditions. This supports the assumption that isotopically light inorganic carbon from deeper water levels of the stratified water body is probably not the only source for isotopically light carbon. Despite this, differences in $\delta^{13}C$ of *n*-alkanes derived from aquatic and terrigenous organisms, suggest that isotopically light carbon influenced the marine before the atmospheric CO_2 pool.

Pristane and phytane show only a small negative isotope excursion (2‰) without depth trend in the T-CIE. As $\delta^{13}C$ of isoprenoids and *n*-alkanes or bulk organic matter are not correlated, it is likely that they reflect a different, yet unidentified CO_2 reservoir.

The Posidonia Shale at Salem is thermally mature and highly oil-prone. PI values are higher and HI values are lower than those in the immature to marginal mature Dormettingen section. The residual source petroleum potential of the cored section is about 0.5 tHC/m^2 and may be 0.8 tHC/m^2 for the entire Posidonia Shale.

Declarations

Conflict of interest All authors declare that they have no conflict of interest.

Ethics approval Not applicable.

Consent to participate Not applicable.

Consent for publication Not applicable.

References

Ajuaba S, Sachsenhofer RF, Galasso F, Bechtel A, Gross D, Misch D, Schneebeli-Hermann E (2022) Biomarker and compound-specific isotope records across the Toarcian CIE at the Dormettingen section in SW Germany. Int J Earth Sci 111:1631–1661. https://doi.org/10.1007/s00531-022-02196-z

Arp G, Gropengießer S, Schulbert C, Jung D, Reimer A (2021) Biostratigraphy and sequence stratigraphy of the Toarcian Ludwigskanal section (Franconian Alb, Southern Germany). Zitteliana 95:57–94. https://doi.org/10.3897/zitteliana.95.56222

Batten DJ (1996) Palynofacies. In: Jansonius J, McGregor DC (eds) Palynology: principles and applications, vol 3. Park Ridge, American Association of Stratigraphy Palynologists Foundation, pp 1011–1064

Baucon A, Bednarz M, Dufour S, Felletti F, Malgesini G, de Carvalho CN, Niklas KJ, Wehrmann A, Batstone R, Bernardini F, Briguglio A, Cabella R, Cavalazzi B, Ferrretti A, Zanzerl H, McIlroy D (2020) Ethology of the trace fossil Chondrites: Form, function and environment. Earth Sci Rev 202:102989. https://doi.org/10.1016/j.earscirev.2019.102989

Baudin F (1995) Depositional controls on Mesozoic source rocks in the Tethys. In: Huc A-Y (ed) Paleogeography, paleoclimate, and source rock, vol 40. American Association of Petroleum Geologists Studies in Geology, Houston, pp 191–211

Bechtel A, Berling M, David P, Dax F, Garlichs TU, Gratzer R, Groß, D, Köhler V, Oriabure JE, Sachsenhofer RF (2019) Oil-source correlation in the German Molasse basin. In: 29th Int. Meeting Org. Geochem. https://doi.org/10.3997/2214-4609.201902720 **(IMOG 2019)**

Bour I, Mattioli E, Pittet B (2007) Nannofacies analysis as a tool to reconstruct paleoenvironmental changes during the Early Toarcian anoxic event. Palaeogeogr Palaeoclimatol Palaeoecol 249:58–79

Bowden SA, Farrimond P, Snape CE, Love GD (2006) Compositional differences in biomarker constituents of the hydrocarbon, resin, asphaltene and kerogen fractions: an example from the Jet Rock (Yorkshire, UK). Org Geochem 37:369–383

Bray EE, Evans ED (1961) Distribution of n-parafins as a clue to recognition of source beds. Geochim Cosmochim Acta 22:2–15

Bromley RG, Ekdale AA (1984) Chondrites: a trace fossil indicator of anoxia in sediment. Science 224:872–874

Bruns B, di Primio R, Berner U, Littke R (2013) Petroleum system evolution in the inverted Lower Saxony Basin, northwest Germany: a 3D basin modeling study. Geofluids 13:246–271. https://doi.org/10.1111/gfl.12016

Burnaz L, Littke R, Grohmann S, Erbacher J, Strauss H, Amann F (2024) Lower Jurassic (Pliensbachian-Toarcian) marine paleoenvironment transition in Western Europe: sedimentology, geochemistry and organic petrology of the wells Mainzholzen and Wickensen, Hils Synline, Lower Saxony Basin. Int J Earth Sci **(in press)**

Caruthers AH, Smith PL, Gröcke DR (2013) The Pliensbachian-Toarcian (Early Jurassic) extinction, a global multi-phased event. Palaeogeogr Palaeoclimatol Palaeoecol 386:104–118. https://doi.org/10.1016/j.palaeo.2013.05.010

Chairi R, Derenne S, Largeau C (2010) Alkylbenzene origin in recent sediments from the hypersaline environment of Moknine Sebkha, Tunisi. Rapp Comm Int Mer Médit 39:233

Chen W, Kemp DB, He T, Newton RJ, Xiong Y, Jenkyns HC, Izumi K, Cho T, Huang C, Poulton SW (2023) Shallow-and deep-ocean Fe cycling and redox evolution across the Pliensbachian-Toarcian boundary and Toarcian Oceanic Anoxic Event in Panthalassa. Earth Planet Sci Lett 602:117959. https://doi.org/10.1016/j.epsl.2022.117959

Demaison G, Huizinga BJ (1994) Genetic classification of petroleum systems using three factors: charge, migration and entrapment. In: Magoon LB, Dow WG (eds) The petroleum system, from source to trap, vol 60. AAPG Memoir, pp 73–89

Dera G, Neige P, Dommergues J-L, Fara E, Laffont R, Pellenard P (2010) High resolution dynamics of Early Jurassic marine extinctions: the case of Pliensbachian-Toarcian ammonites (Cephalopoda). J Geol Soc Lond 167:21–33. https://doi.org/10.1144/0016-76492009-068

Derenne S, Largeau C, Casadevall E, Sinninghe-Damsté JS, Tegelaar EW, de Leeuw JW (1990) Characterisation of Estonian Kukersite by spectroscopy and pyrolysis: evidence for abundant alkyl phenolic moieties in an Ordovician, marine, Type II/I kerogen. Org Geochem 16:873–888

Didyk B, Simoneit B, Brassell S, Eglinton G (1978) Organic geochemical indicators of palaeoenvironmental conditions of sedimentation. Nature 272:216–222

Eglinton G, Hamilton R (1967) Leaf epicutular waxes. Science 156:1322–1335

Espitalié J, Laporte JL, Madec M, Marquis F, Leplat P, Paulet J, Boutefeu A (1977) Méthode rapide de caractérisation des roches mètres, de leur potentiel pétrolier et de leur degré d'éevolution. Rev L'institut Français Du Pétrole 32:23–42. https://doi.org/10.2516/ogst:1977002

Fantasia A, Adatte T, Spangenberg JE, Font E, Duarte LV, Follmi KB (2019) Global versus local processes during the Pliensbachian-Toarcian transition at the Peniche GSSP, Portugal: a multi-proxy record. Earth-Sci Rev 1:1. https://doi.org/10.1016/j.earscirev.2019.102932

Fernandez A, Korte C, Ullmann CV, Looser N, Wohlwend S, Bernasconi SM (2021) Reconstructing the magnitude of Early Toarcian (Jurassic) warming using the reordered clumped isotope compositions of belemnites. Geochim Cosmochim Acta 293:308–327. https://doi.org/10.1016/j.gca.2020.10.005

French KL, Sepulveda J, Trabucho-Alexandre J, Gröcke DR, Summons RE (2014) Organic geochemistry of the early Toarcian oceanic anoxic event in Hawsker Bottoms, Yorkshire, England. Earth Planet Sci Lett 390:116–127. https://doi.org/10.1016/j.epsl.2013.12.033

Frimmel A, Oschmann W, Schwark L (2004) Chemostratigraphy of the Posidonia Black Shale, SW Germany I. Influence of sea-level variation on organic facies evolution. Chem Geol 206:199–230

Fu S (1991) Funktion, Verhalten und Einteilung fucoider und lophocteniider Lebensspuren. Courier Forschungsinst Senckenberg 135:64

Galasso F, Schmid-Röhl A, Feist-Burkhardt S, Bernasconi SM, Schneebeli-Hermann E (2021) Changes in organic matter composition during the Toarcian Oceanic Anoxic Event (T-OAE) in the Posidonia Shale Formation from Dormettingen (SW-Germany). Palaeogeogr Palaeoclimatol Palaeoecol 569:110327. https://doi.org/10.1016/j.palaeo.2021.110327

Galasso F, Feist-Burkhardt S, Schneebeli-Hermann E (2022) The palynology of the Toarcian Oceanic Anoxic Event at Dormettingen, southwest Germany, with emphasis on changes in vegetational dynamics. Rev Palaeobot Palynol 304:104701. https://doi.org/10.1016/j.revpalbo.2022.104701

Goodwin NS, Mann AL, Patience RL (1988) Structure and significance of C30 4-methylsteranes in lacustrine shales and oils. Org Geochem 12:495–506

Grice K, Schouten S, Peters KE, Sinninghe Damsté JS (1998) Molecular isotopic characterisation of hydrocarbon biomarkers in Palaeocene-Eocene evaporitic, lacustrine source rocks from the Jianghan Basin, China. Org Geochem 29:1745–1764

Grice K, de Mesmay R, Glucina A, Wang S (2008) An improved and rapid 5A molecular sieve method for gas chromatography isotope ratio mass spectrometry of n-alkanes (C8–C30+). Org Geochem 39:284–288. https://doi.org/10.1016/j.orggeochem.2007.12.009

Harries PJ, Little CTS (1999) The early Toarcian (Early Jurassic) and Cenomanian-Turonian (Late Cretaceous) mass extinctions: similarities and contrasts. Palaeogeogr Palaeoclimatol Palaeoecol 154:39–66. https://doi.org/10.1016/S0031-0182(99)00086-3

Hermoso M, Minoletti F, Le Callonnec L, Jenkyns HC, Hesselbo SP, Rickaby REM, Renard M, de Rafélis M, Emmanuel L (2009) Global and local forcing of Early Toarcian seawater chemistry: a comparative study of different paleoceanographic settings (Paris and Lusitanian basins). Paleoceanography 24:1–15. https://doi.org/10.1029/2009PA001764

Hermoso M, Minoletti F, Pellenard P (2013) Black shale deposition during Toarcian super-greenhouse driven by sea level. Clim past 9(2703):2712

Hermoso M, Delsate D, Baudin F, Le Callonnec L, Minoletti F, Renard M, Faber A (2014) Record of Early Toarcian carbon cycle perturbations in a nearshore environment: the Bascharage section (easternmost Paris Basin). Solid Earth 5:793–804. https://doi.org/10.5194/se-5-793-2014

Hesselbo SP, Gröcke DR, Jenkyns HC, Bjerrum CJ, Farrimond P, Morgans Bell HS, Green OR (2000) Massive dissociation of gas hydrate during a Jurassic oceanic anoxic event. Nature 406:392–395. https://doi.org/10.1038/35019044

Hesselbo SP, Jenkyns HC, Duarte LV, Oliveira LCV (2007) Carbon-isotope record of the Early Jurassic (Toarcian) Oceanic Anoxic Event from fossil wood and marine carbonate (Lusitanian Basin, Portugal). Earth Planet Sci Lett 253:455–470

Hollander DJ, Bessereau G, Belin S, Huc AY, Houzay JP (1991) Organic matter in the early Toarcian shales, Paris Basin, France: a response to environmental changes. Reve De L'institut Francais Du Petrole 46:543–562

Hougård IW, Bojese-Koefoed JA, Vickers ML, Ullmann CV, Bjerrum CJ, Rizzi M, Korte C (2021) Redox element record shows that environmental perturbations associated with the T-OAE were of longer duration than the carbon isotope record suggests – the Aubach section, SW Germany. Newsl Stratigr 54:229–246

Hughes WB, Holba AG, Dzou LIP (1995) The ratios of dibenzothiophene to phenanthrene and pristane to phytane as indicators of

depositional environment and lithology of petroleum source rocks. Geochim Cosmochim Acta 59:3581–3598. https://doi.org/10.1016/0016-7037(95)00225-O

ICCP (1998) The new vitrinite classification (ICCP System 1994). Fuel 77:349–358. https://doi.org/10.1016/S0016-2361(98)80024-0

ICCP (2001) The new inertinite classification (ICCP System 1994). Fuel 80:459–471. https://doi.org/10.1016/S0016-2361(00)00102-2

Izumi K (2012) Formation process of the trace fossil *Phymatoderma granulata* in the Lower Jurassic black shale (Posidonia Shale, southern Germany) and its paleoeco logical implications. Palaeogeogr Palaeoclimatol Palaeoecol 353–355:116–122

Jenkyns HC (1985) The early Toarcian and Cenomanian-Turonian Anoxic Events in Europe: comparisons and contrasts. Geol Rundsch 74:505–518

Jenkyns HC (1988) The early Toarcian (Jurassic) anoxic event: stratigraphic, sedimentary, and geochemical evidence. Am J Sci 288:101–151

Jenkyns HC (2010) Geochemistry of oceanic anoxic events. Geochem Geophys Geosyst 11:1–30. https://doi.org/10.1029/2009GC002788

Jenkyns HC, Clayton CJ (1997) Lower Jurassic epicontinental carbonates and mudstones from England and Wales: chemostratigraphic signals and the early Toarcian anoxic event. Sedimentology 44:687–706. https://doi.org/10.1046/j.1365-3091.1997.d01-43.x

Jenkyns HC, Gröcke DR, Hesselbo SP (2001) Nitrogen isotope evidence for water mass denitrification during the early Toarcian (Jurassic) oceanic anoxic event. Paleoceanography 16:593–603

Kemp DB, Coe AL, Cohen AS, Schwark L (2005) Astronomical pacing of methane release in the Early Jurassic period. Nature 437:396–399. https://doi.org/10.1038/nature04037

Kemp DB, Coe AL, Cohen AS, Weedon GP (2011) Astronomical forcing and chronology of the early Toarcian (Early Jurassic) oceanic anoxic event in Yorkshire. UK Palaeogeogr Palaeoclimatol Palaeoecol 530:90–102

Kuhn O, Etter W (1994) Der Posidonienschiefer der Nordschweiz: lithostratigraphie, Biostratigraphie. Fazies Eclogae Geol Helv 87(1):113–138

Küspert W (1982) Environmental change during oil shale deposition as deduced from stable isotope ratios. In: Einsele S, Seilacher A (eds) Cyclic and event stratification. Springer, New York, pp 482–501

Leythaeuser D, Schaefer RG, Yukler A (1982) Role of diffusion in primary migration of hydrocarbons. AAPG Bull 66:408–429

Littke R, Baker DR, Leythaeuser D, Rullkotter J (1991a) Keys to the depositional history of the Posidonia Shale (Toarcian) in the Hils Syncline, northern Germany. In: Tyson RV, Pearson TH (eds) Modern and ancient continental shelf anoxia, special publications, vol 58. Geological Society, London, p 311. https://doi.org/10.1144/GSL.SP.1991.058.01.20

Littke R, Rotzal H, Leythaeuser D, Baker DR (1991b) Lower Toarcian Posidonia Shale in Southern Germany (Schwaebische Alb). Organic facies, depositional environment and maturity. Erdöl Kohle Erdgas Petrochem Hydrocarb Technol 44:407–414

Mackenzie AS, Maxwell JR (1981) Assessment of thermal maturation in sedimentary rocks by molecular measurements. In: Brooks J (ed) Organic maturation studies and fossil fuel exploration. Academic Press, London, pp 239–254

Mattioli E, Pittet B, Suan G, Mailliot S (2008) Calcareous nannoplankton changes across the early Toarcian oceanic anoxic event in the Western Tethys. Paleoceanography 23:PA3208. https://doi.org/10.1029/2007PA001435

McElwain JC, Wade-Murphy J, Hesselbo SP (2005) Changes in carbon dioxide during an oceanic anoxic event linked to intrusion into Gondwana coals. Nature 435(7041):479–482

McNeil RI, BeMent WO (1996) Thermal stability of hydrocarbons: laboratory criteria and field examples. Energy Fuel 10:6067

Meyer RKF, Schmidt-Kaler H (1996) Jura. In: Freudenberger W, Schwerd K (eds) Erläuterungen zur geologischen karte von Bayern 1:500,000, 4th edn. Bayrisches Geologisches Landesamt, München, pp 90–111

Misch D, Leu W, Sachsenhofer RF, Gratzer R, Rupprecht B, Bechtel A (2017) Shallow hydrocarbon indications along the Alpine thrust belt and adjacent foreland basin: distribution and implications for petroleum exploration. J Petrol Geol 40:341–362

Moldowan JM, Talyzina NM (1998) Biogeochemical evidence for dinoflagellate ancestors in the Early Cambrian. Science 281:1168–1170

Montero-Serrano J-C, Föllmi KB, Adatte T, Spangenberg JE, Tribovillard N, Fantasia A, Suan G (2015) Continental weathering and redox conditions during the early Toarcian Oceanic Anoxic Event in the northwestern Tethys: insight from the Posidonia Shale section in the Swiss Jura Mountains. Palaeogeogr Palaeoclimatol Palaeoecol 429:83–99. https://doi.org/10.1016/j.palaeo.2015.03.043

Noble RA, Alexander R, Kagi RI, Knox J (1986) Identification of some diterpenoid hydrocarbons in petroleum. Org Geochem 10:825–829

Pálfy J, Smith PL (2000) Synchrony between Early Jurassic extinction, oceanic anoxic event, and the Karoo-Ferrar flood basalt volcanism. Geology 28:747–750. https://doi.org/10.1130/0091-7613(2000)028%3c0747:SBEJEO%3e2.3.CO;2

Pedentchouk N, Turich C (2017) Carbon and hydrogen isotopic compositions of n-alkanes as a tool in petroleum exploration. Hydrocarbon Syst Geol Soc Lond Spec Publ 468:105–125. https://doi.org/10.1144/SP468.1

Peters KE (1986) Guidelines for evaluating petroleum source rock using programmed pyrolysis. AAPG Bull Am Assoc Pet Geol 70(3):318–329. https://doi.org/10.1306/94885688-1704-11D7-8645000102C1865D

Peters KE, Moldowan JM (2001) Effects of source, thermal maturity, and biodegradation on the distribution and isomerization of homohopanes in petroleum. Org Geochem 17:47–61

Peters KE, Walters CC, Moldowan JM (2005) The biomarker guide: biomarkers and isotopes in petroleum systems and earth history, 2nd edn. Cambridge University Press, Cambridge

Pickel W, Kus J, Flores D, Kalaitzidis S, Christanis K, Cardott BJ, Misz-Kennan M, Rodrigues S, Hentschel A, Hamor-Vido M, Crosdale P, Wagner N, ICCP (2017) Classification of liptinite–ICCP System (1994). Int J Coal Geol 169:40–61. https://doi.org/10.1016/j.coal.2016.11.004

Prauss M (1996) The Lower Toarcian Posidonia Shale of Grimmen, Northeast Germany. Implications from the palynological analysis of a near-shore section. Neues Jahrb Für Geol Paläontol Abh 200:107–132

Prauss M, Riegel W (1989) Evidence from phytoplankton associations for causes of black shale formation in epicontinental seas. Neues Jb Geol Paläontol Monat 11:671–682

Prauss M, Ligouis B, Luterbacher H (1991) Organic matter and palynomorphs in the 'Posidonienschiefer' (Toarcian, lower Jurassic) of southern Germany. Geol Soc Lond Spec Publ 58:335–351

Radke M (1988) Application of aromatic compounds as maturity indicators in source rocks and crude oils. Mar Petrol Geol 5:224–236

Radke M, Willsch H, Welte DH (1980) Preparative hydrocarbon group type determination by automated medium pressure liquid chromatography. Anal Chem 52:406–411

Radke M, Welte DH, Willsch H (1986) Maturity parameters based on aromatic hydrocarbons: Influence of the organic matter type. Org Geochem 10:51–63

Riegraf W (1985) Mikrofauna, biostratigraphie und fazies im unteren toarcium sudwestdeutschlands und vergleiche mit benachbarten gebieten. Tub Mikropaläont Mitt 3:232

Riegraf W, Werner G, Lörcher F (1984) Der Posidonienschiefer—biostratigraphie, Fauna und Fazies des südwestdeutschen Untertoarciums (Lias ε). Enke, Stuttgart, p 195

Röhl H-J, Schmid-Röhl A, Oschmann W, Frimmel A, Schwark L (2001) Erratum to "The Posidonia Shale (Lower Toarcian) of SW-Germany: an oxygen-depleted ecosystem controlled by sea level and palaeoclimate." Palaeogeogr Palaeoclimatol Palaeoecol 169:273–299

Röhl H-J, Schmid-Röhl A (2005) Lower Toarcian (Upper Liassic) black shales of the Central European Epicontinental Basin: a sequence stratigraphic case study from the SW German Posidonia Shale. In: The deposition of organic-carbon-rich sediments: models, mechanisms, and consequences, vol 82. SEPM (Society for Sedimentary Geology) Spec. Publ, pp 165–189

Ruebsam W, Al-Husseini M (2020) Calibrating the Early Toarcian (Early Jurassic) with stratigraphic black holes (SBH). Gondwana Res 82:317–336. https://doi.org/10.1016/j.gr.2020.01.011

Ruebsam W, Schwark L (2021) Impact of a northern-hemispherical cryosphere on late Pliensbachian–early Toarcian climate and environment evolution. Geol Soc Lond Spec Publ 514:359–385. https://doi.org/10.1144/SP514-2021-11

Ruebsam W, Mayer B, Schwark L (2019) Cryosphere carbon dynamics control early Toarcian global warming and sea level evolution. Global Planet Change 172:440–453. https://doi.org/10.1016/j.gloplacha.2018.11.003

Ruebsam W, Schmid-Röhl A, Al-Husseini M (2023) Astronomical timescale for the early Toarcian (Early Jurassic) Posidonia Shale and global environmental changes. Palaeogeogr Palaeoclimatol Palaeoecol 623:111619

Sachsenhofer RF, Leitner B, Linzer H-G, Bechtel A, Ćorić S, Gratzer R, Reischenbacher D, Soliman A (2010) Deposition, erosion and hydrocarbon source potential of the oligocene eggerding formation (Molasse Basin, Austria). Aust J Earth Sci 103:76–99

Schlanger SO, Jenkyns HC (1976) Cretaceous oceanic anoxic events: causes and consequences. Geologieenmijnbouw 55(3–4):179–184

Schmid-Röhl A, Röhl H-J, Oschmann W, Frimmel A, Schwark L (2002) Palaeoenvironmental reconstruction of Lower Toarcian epicontinental black shales (Posidonia Shale, SW Germany): global versus regional control. Geobios 35:13–20

Schouten S, van Kaam-Peters HME, Rijpstra WIC, Schoell M, Sinninghe Damste JS (2000) Effects of an oceanic anoxic event on the stable carbon isotopic composition of early Toarcian carbon. Am J Sci 300:1–22

Schulz H-M, Sachsenhofer RF, Bechtel A, Polesny H, Wagner L (2002) The origin of hydrocarbon source rocks in the Austrian Molasse Basin (Eocene-Oligocene transition). Mar Pet Geol 19:683–709

Schwark L, Frimmel A (2004) Chemostratigraphy of the Posidonia Black Shale, SW Germany II. Assessment of extent and persistence of photic-zone anoxia using aryl isoprenoid distribution. Chem Geol 206:231–248

Seifert WK, Moldowan JM (1986) Use of biological markers in petroleum exploration. In: Johns RB (ed) Methods in geochemistry and geophysics, vol 24. Elsevier, Amsterdam, pp 261–290

Seilacher A (1990) Aberration in bivalve evolution related to photo- and chemosymbiosis. Hist Biol 3:289–311. https://doi.org/10.1080/08912969009386528

Sinninghe Damsté J, Kenig F, Koopmans M, Köster J, Schouten S, Hayes J, de Leeuw J (1995) Evidence for gammacerane as an indicator of water column stratification. Geochim Cosmochim Acta 59:1895–1900

Sinninghe-Damsté JS, Keely BJ, Betts SE, Baas M, Maxwell JR, de Leeuw JW (1993) Variations in abundances and distributions of isoprenoid chromans and longchain aikylbenzenes in sediments of the Mulhouse Basin: a molecular sedimentary record of palaeosalinity. Org Geochem 20:1201–1215

Song J, Littke R, Maquil R, Weniger P (2014) Organic facies variability in the Posidonia Black Shale from Luxembourg: implications for thermal maturation and depositional environment. Palaeogeogr Palaeoclimatol Palaeoecol 410:316–336

Song J, Littke R, Weniger P, Ostertag-Henning C, Nelskamp S (2015) Shale oil potential and thermal maturity of the Lower Toarcian Posidonia Shale in NW Europe. Int J Coal Geol 150–151:127–153

Song J, Littke R, Weniger P (2017) Organic geochemistry of the Lower Toarcian Posidonia Shale in NW Europe. Org Geochem 106(2017):76–92

Stock AT, Littke R (2018) The Posidonia Shale of northern Germany: unconventional oil and gas potential from high-resolution 3D numerical basin modelling of the cross-junction between the eastern Lower Saxony Basin, Pompeckj Block and Gifhorn Trough. In: Kilhams B, Kukla PA, Mazur S, McKie T, Mijnlieff HF, Van Ojik K (eds) Mesozoic Resource Potential in the Southern Permian Basin, vol 469. Geological Society, London Special Publications, London, pp 399–421

Suan G, Pittet B, Bour I, Mattioli E, Duarte LV, Mailliot S (2008) Duration of the Early Toarcian carbon isotope excursion deduced from spectral analysis: consequence for its possible causes. Earth Planet Sci Lett 267:666–679

Suan G, van de Schootbrugge B, Adatte T, Fiebig J, Oschmann W (2015) Calibrating the magnitude of the Toarcian carbon cycle perturbation. Paleoceanography 30:495–509. https://doi.org/10.1002/2014PA002758

Summons RE, Powell TG (1987) Identification of aryl isoprenoids in source rocks and crude oils: Biological markers for the green sulphur bacteria. Geochim Cosmochim Acta 51:557–566

Svensen H, Planke S, Chevallier L, Malthe-Sørenssen A, Corfu F, Jamtveit B (2007) Hydrothermal venting of greenhouse gases triggering Early Jurassic global warming. Earth Planet Sci Lett 256:554–566

Taylor G, Teichmüller M, Davies A, Diessel D, Littke R, Robert P (1998) Organic petrology: a new handbook incorporation some revised parts of stach's textbook of coal petrology. Gebrüder Borntraeger, Berlin

Them TR II, Gill BC, Caruthers AH, Gröcke DR, Tulsky ET, Martindale RC, Poulton TP, Smith PL (2017) High-resolution carbon isotope records of the Toarcian Oceanic Anoxic Event (Early Jurassic) from North America and implications for the global drivers of the Toarcian carbon cycle. Earth Planet Sci Lett 459:118–126. https://doi.org/10.1016/j.epsl.2016.11.021

Traverse A (2007) Paleopalynology. Topics in geobiology, vol 28. Springer, Dordrecht

Tyson RV (1995) Sedimentary organic matter—organic facies and palynofacies. Chapman and Hall, London

Uchman A, Wetzel A (1999) An aberrant, helicoidal trace fossil Chondrites Sternberg. Palaeogeogr Palaeoclimatol Palaeoecol 146:165–169. https://doi.org/10.1016/S0031-0182(98)00148-5

van Acken D, Tütken T, Daly JS, Schmid-Röhl A, Orr PJ (2019) Rhenium-osmium geochronology of the Toarcian Posidonia Shale, SW Germany. Palaeogeogr Palaeoclimatol Palaeoecol 534:109294

Van de Schootbrugge B, McArthur JM, Bailey TR, Rosenthal Y, Wright JD, Miller KG (2005) Toarcian oceanic anoxic event: an assessment of global causes using belemnite C isotope records. Paleoceanography 20:1-10 PA3008. https://doi.org/10.1029/2004PA001102

Van de Schootbrugge B, Richoz S, Pross J, Luppold FW, Hunze S, Wonik T, Blau J, Meister C, van der Weijst CMH, Suan G, Fraguas A, Fiebig J, Herrle JO, Guex J, Little CTS, Wignall PB,

Püttmann W, Oschmann W (2019) The Schandelah Scientific Drilling Project: a 25-million year record of Early Jurassic palaeoenvironmental change from northern Germany. Newsl Stratigr 52(3):249–296. https://doi.org/10.1127/nos/2018/0259

Veron J (2005) The Alpine Molasse basin—review of petroleum Geology and remaining potential. Bull Angew Geol 10:75–86

Volkman JK, Kearney P, Jeffrey SW (1990) A new source of 4-methyl and 5α(H)-stanols in sediments: prymnesiophyte microalgae of the genus *Pavlova*. Org Geochem 15:489–497

Wang Y, Ossa Ossa F, Wille M, Schurr S, Saussele M, Schmid-Röhl A, Schoenberg R (2020) Evidence for local carbon-cycle perturbations superimposed on the Toarcian carbon isotope excursion. Geobiology 18:682–709. https://doi.org/10.1111/gbi.12410

Wang Y, Ossa Ossa F, Spangenberg JE, Wille M, Schoenberg R (2021) Restricted oxygen-deficient basins on the Northern European epicontinental shelf across the Toarcian carbon isotope excursion interval. Paleoceanogr Paleoclimatol 36:e2020PA004207. https://doi.org/10.1029/2020PA004207

Wehner H, Kuckelkorn K (1995) Zur Herkunft der Erdöle im nördlichen Alpen- /Karpatenvorland. Erdöl Erdgas Kohle 111:508–514

Withers N (1987) Dinoflagellate sterols. In: Taylor FJR (ed) The biology of dinoflagelltes. Blackwell Scientific, Oxford, pp 316–359

Yule B, Roberts S, Marshall JEA, Milton JA (1998) Quantitative spore colour measurement using colour image analysis. Org Geochem 28:139–149

Zhang YD, Jiang AZ, Sun YG, Xie LJ, Chai PX (2012) Stable carbon isotope compositions of isoprenoid chromans in cenozoic saline lacustrine source rocks from the Western Qaidam Basin, NW China: source implications. Chin Sci Bull 57:560–570

Zheng T, Grohmann S, Arysanto A, Baniasad A, Zhang Q, Littke R (2023) Petrographical and geochemical investigations on maturation and primary migration in intact source rock micro-plugs: Insight from hydrous pyrolysis on Woodford Shale. Int J Coal Geol 266:104170

Ziegler PA (1982) Geological Atlas of Central and Western Europe. Shell International Petroleum Maatschappij BV, Amsterdam, p 130

Ziegler PA (1988) Evolution of the Arctic-North Atlantic and the Western Tethys. Am Assoc Petrol Geol Mem 43:197

Ziegs V, Horsfield B, Skeie JE, Rinna J (2017) Petroleum retention in the Mandal Formation, Central Graben, Norway. Mar Pet Geol 83:195–214